Biochemical Characterization and Inhibition of Influenza B Virus RNA-Dependent RNA Polymerase

by

Parisa Raeisimakiani

A thesis submitted in partial fulfillment of the requirements for the degree of

Master of Science

in

Virology

Department of Medical Microbiology and Immunology

University of Alberta

Abstract

The influenza virus can cause severe respiratory illness in humans and animals. There are four types of influenza viruses (A, B, C, and D); however, only type A and B cause severe diseases in humans. Influenza virus belongs to the family *Orthomyxoviridae*, which includes segmented negative-sense RNA viruses. The Influenza RNA-dependent RNA polymerase (RdRp) is responsible for both viral genome replication and transcription. RdRp functions are essential to the viral life cycle, suggesting that it is a logical target for antiviral drugs. The RdRp is a heterotrimeric protein consisting of a catalytically active polymerase subunit (PB1), an endonuclease subunit (PA), and a cap-binding subunit (PB2).

In this study, we purified influenza B RdRp and studied inhibitors of PB1 and PA. Favipiravir is a drug that targets PB1. This compound is a purine analog that affects RNA synthesis. Recent *in vitro* selection experiments revealed resistance-conferring mutations in the RdRp complex. We developed biochemical assays to elucidate the underlying mechanisms associated with inhibition and resistance. We demonstrated that the mutant enzyme diminishes rates of incorporation of the inhibitor when compared with the wild type. We have also identified structurally distinct nucleotide analogue inhibitors of RdRp that are not affected by this mutation. Thus, the mechanism of resistance seems to be specific. Baloxavir targets the endonuclease subunit PA. The influenza RdRp complex possesses two active sites that contain two divalent metal ions: the polymerase active site in PB1 and the endonuclease active site in PA. Using the purified RdRp complex, we utilized RNA polymerization and endonuclease assays to test selected compounds

for potential inhibitory effects. The data shows that Baloxavir is a selective endonuclease inhibitor, and RNA synthesis is solely affected at very high concentrations of the inhibitor. The collective data confirms that targeting the polymerase and endonuclease active sites is a feasible approach. Future studies will show whether novel therapies based on these types of drug combinations may improve clinical outcomes.

Preface

Portion of chapter 3 specifically figure 3.1.3 and table 3.1 have been previously published as E. P. Tchesnokov, **P. Raeisimakiani**, M. Ngure, D. Marchant, and M. Götte, "Recombinant RNA-Dependent RNA Polymerase Complex of Ebola Virus," *Sci. Rep.*, vol. 8, no. 1, pp. 1–9, 2018 [1].

Construct design and expression of influenza RdRp was established by Dr. Egor Tchesnokov in our laboratory [1]. All endonuclease assays, graph figure 4.4, and values obtained from endonuclease assays in table 4.1 were done by Brendan Todd. All other experimentation and analysis were completed by myself.

Dedicated to my mom and dad

Mahboobeh and Javad

For their love and support

Acknowledgments

This work would not have been done without the endless support and input of my project supervisor Dr. Matthias Götte. Words cannot describe his enormous help and ease he provided me to complete this work. I would like to thank Dr. Edan Foley for all his support and precise help while writing this thesis. Edan, the mental support you provided was undoubtedly unforgettable and had a great role in the completion of this thesis. I also want to thank my supervisory committee members Dr. Kathy Magor and Dr. David Marchant for their time and feedback on my research progress.

I would also like to thank Dr. Egor Tchesnokov for his knowledge and enthusiasm for science. I am thankful for all the discussions we had before and after each experiment. I benefitted the most from his technical suggestions, and he made this journey smoother for me. I am blessed to have Brendan Todd as my labmate and good friend, for all his generous feedback, the effort and support during writing this thesis. I would also want to thank all members of the Götte Lab, past and present.

I very much appreciate the help of all the administrative staff of Medical Microbiology and Immunology. The hidden part of each and every experiment which conducts in the MMI labs. In particular, I would like to thank Tabitha Vasquez and Debbie Doudiet and Michelle Zadunayski.

I would also want to thank my dear friends, friends who are family, Saeideh Davoodi and Marzieh Kooshkbaghi, for all their support and love throughout the years that made my life happier away from the family. Last but not least, I would like to thank my best friend and partner, Abolfazl Ashrafi, for all his support and love that warms my heart. I am thankful for his good energy, which is always encouraging.

Table of Contents

List of Tables

List of Figures

List of Abbreviations

°C	Degrees Celsius
µg	Microgram
µl	Microliter
µM	Micromolar
%	Percent
ATP	Adenosine triphosphate
BXA	Baloxavir Acid
CDC	Center for Disease and prevention
CTP	Cytosine triphosphate
CV	Column Volume
CVB3	coxsackievirus B3
EDTA	Ethylenediaminetetraacetic acid
ER	Endoplasmic reticulum
FDA	Food and Drug Administration
GTP	Guanosine triphosphate
HA	Hemagglutinin
HIV	Human Immune deficiency Virus
IC50	Half Maximal Inhibitory Concentration
IPTG	Isopropyl β-D-1-thiogalactopyranoside
LAIV	Live attenuated influenza vaccine
MDCK	Madin-Darby Canine Kidney cells
MS	Mass Spectrometry
MW	Molecular Weight
mM	Millimolar
NA	Neuraminidase
NAI	Neuraminidase Inhibitor
nm	nanometer
NP	Nuclear Protein

NTP	Nucleoside triphosphate
PA	Polymerase Acidic
PAGE	Polyacrylamide gel electrophoresis
PB1	Polymerase Basic 1
PB2	Polymerase Basic 2
PDB	Protein Data Bank
RCF	Relative Centrifugal Force
RFU	Relative Fluorescence Unit
RNA	Ribonucleic acid
RNP	Ribonucleoprotein
F-RTP	Favipiravir- ribofuranosyl 5’-triphosphate
SDS	Sodium Dodecyl Sulfate
SF9	Spodoptera frugiperda
TCEP	Tris-2-carboxyethylphosphine
TEV	Tobacco Etch Virus
mTOC	microtubule-organizing center
UTP	Uridine triphosphate
WHO	World Health Organization
WT	Wild Type
YFP	Yellow Fluorescent Unit

Chapter 1. Introduction

1.1 Introduction to Influenza Virus

1.1.1 History

The influenza A and B virus or Flu causes a highly contagious acute respiratory infection in humans and animals [2], [3]. Influenza A is responsible for occasional pandemic and it is divided into subtypes based on surface proteins, H and N. On the other hand, influenza B is responsible for yearly epidemic and it is classified into two different genetic lineages: Yamagata and Victoria. The first detailed report on Influenza infection, which was recorded in 1850, spread into three continents of Asia, Europe and Africa [4]

Since then, within the last 170 years, seven influenza pandemics have occurred. Another pandemic occurred in 1889. however, the most notorious pandemic, referred to as the "Spanish flu", caused by influenza A (H1N1), has been linked to 50 to 100 million deaths worldwide [5]. The next pandemic that occurred in 1957 and was called "Asian flu" was caused by the H2N2 subtype and killed two million people. During the "Hong Kong flu" pandemic in 1968, Influenza A(H3N2) caused another pandemic that claimed 1 million lives. Again, in 1977, Influenza A(H1N1) caused the sixth recorded pandemic.

The last Influenza pandemic occurred in June 2009 and is also known as the first pandemic of the 21st century. The pandemic was caused by influenza A(H1N1). It started in Mexico and spread worldwide. 214 countries reported confirmed deaths because of influenza A(H1N1) infection. A total number of 150,000 death worldwide [6] and almost 450 deaths related to influenza infection in Canada was reported.

The influenza virus is zoonotic, and waterfowls are their first reservoir [7]. The disease is usually asymptomatic in birds; however, it can appear as mild to acute as well, and it can infect both the upper and lower respiratory tract [7]. The symptoms include cough, fever, musculoskeletal, ocular manifestation, renal and other organ diseases [8], [9]. Influenza infection imposes a high financial and health burden, as it approximately causes 12,200 hospitalizations and 3,500 deaths in Canada, annually [10].

1.1.2 Classification

The influenza virus belongs to the *Orthomyxoviridae* (ortho means "straight," and myxo means "mucus") family [11]. They are single-stranded RNA negative sense viruses that consist of seven genera: Influenza A, B, C, D, Isavirus, Thogotovirus and Quaranjavirus. Influenza A is responsible for infection in birds and mammals, and Influenza B causes disease in humans and seals [12]. Influenza C infects humans and pigs [13], and Influenza D is known to infect only pigs and cattles. Isavirus causes infection in fish, such as salmon, and Thogotovirus infects ticks, sea lice and mosquitoes, as well as vertebrates, such as mice and hamsters. The last member of the family, Quaranjavirus, causes infection in humans, ticks and seabirds [14].

There are three types of human influenza viruses: A, B, and C. The accepted nomenclature for influenza consists of 1) the type; 2) the location it is isolated; 3) number of isolation; and 4) the year it has been isolated. Additionally, in the case of influenza A, the subtypes of the two surface glycoproteins, Neuraminidase (NA) and Hemagglutinin (HA) are also included [15], [16]. As of now, 9 NA (N1 to N9) subtypes and 17 HA (H1 to H17) subtypes have been identified, and together it gives a potential of 153 combinations [15], [17]. Influenza pandemics occur when

Influenza A breaks cross-species barriers and result in a newly emerged virus. The new virus possesses a high rate of mortality and morbidity due to a lack of host immune memory [7]. influenza B is only responsible for seasonal epidemics with a lower rate of mortality [18]–[21].

1.1.3 Virion structure

The influenza virion structure is similar in all three types of human influenza. They are spherical, with a diameter between 80-120 nm [22]. They are enveloped with the lipid bilayer, budded from the host cell [23]. There are two major surface glycoproteins, Neuraminidase (NA) and Hemagglutinin (HA), that are necessary for viral entry and release (Figure 1.1-A). Matrix 1 (M1) protein is located underneath the lipid-bilayer, and it is responsible for the shape and structure of the virus. However, Matrix 2 (M2) protein is an ion channel and is responsible for viral RNA released into the host cell cytoplasm. It is important to note that the M2 ion channels are specific to influenza. The virus of influenza B lacks this protein [24], [25].

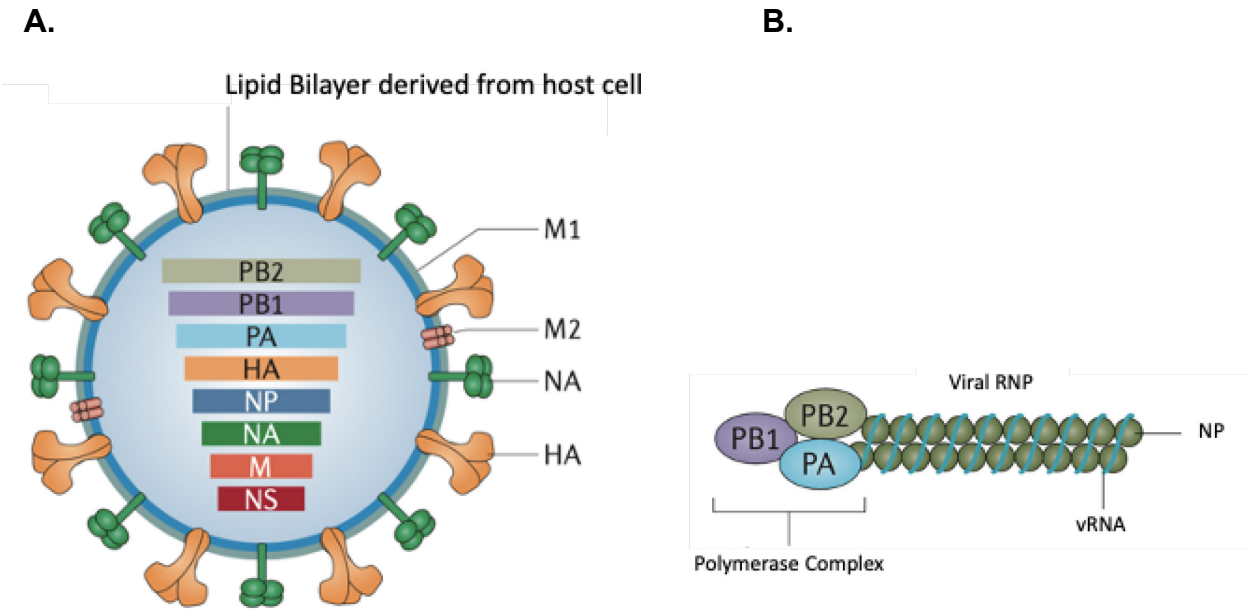

Figure 1.1: Schematic shows the structure of Influenza A virus and vRNP layout. Figure adapted from Shi et al, 2014 [26]. (A) The figure shows the arrangement of the influenza virus lipid bilayer, surface protein and segmented genes. (B) Viral RNP.

The genome is comprised of 8 segments in influenza A, B and seven segments in influenza C encodes for different proteins, as shown in figure 1-A. Highly conserved 3' and 5' termini of each segment partially anneal, and one RNA-dependent RNA polymerase (RdRp) binds to this structure. The remaining vRNA is covered by Oligomeric Nucleoproteins (NPs) (Figure 1.1-B).

1.2 Cell Cycle

1.2.1 Cell entry and release of the vRNA to the cytoplasm

The cycle starts by attaching sialic acid on the surface of the host cell-mediated by hemagglutinin. The internalization of the virion occurs through endocytosis and mainly through Clathrin-mediated endocytosis [27]. After fusion and internalization of the virion, the M2 ion channels

open and allow for the flow of the hydrogen ion inside the virion. The high concentration of hydrogen ions results in acidification of the endocytosed virion and ultimately causes the un-coating of the vRNP into the cell cytoplasm. The eight vRNP are transferred to the nucleus facilitated by the Nuclear Localization Signal on the nucleoprotein for further transcription and replication [28].

1.2.2 Replication and Transcription of the vRNA

RNA-dependent RNA polymerase of influenza virus is responsible for both replication and transcription of the virus; however, different conformational changes are required. RdRp of influenza virus is a heterotrimeric protein, and each subunit has an assigned role; Polymerase Basic 1 (PB1) is the catalytic domain of the protein, Polymerase basic 2 (PB2) is the primer binding domain, and the Polymerase Acidic (PA) is the endonuclease domain (Figure 1.2). Influenza virus transcription is 5' capped-primer dependent. However, the influenza virus lacks a process synthesis of its own 5' capped-primer; therefore, the virus uses a mechanism called cap-snatching. PB2 subunit recognizes and binds to the host capped mRNA; then the PA subunit, which possesses the endonuclease activity, cleaves and hijacks approximately 10-15 nucleotides downstream of the host capped mRNA [29]. PA subunit, then, rotates and brings the free 3' hydroxyl to the active site of the PB1 subunit, and RNA synthesis takes place. Unlike transcription, replication is primer-independent and is known to be de novo. During replication, the RdRp of influenza virus uses the viral RNA to synthesize complementary RNA (cRNA), which is a positive-strand RNA. Influenza RdRp uses cRNA as a template to synthesis vRNA [30], [31], [32], [45].

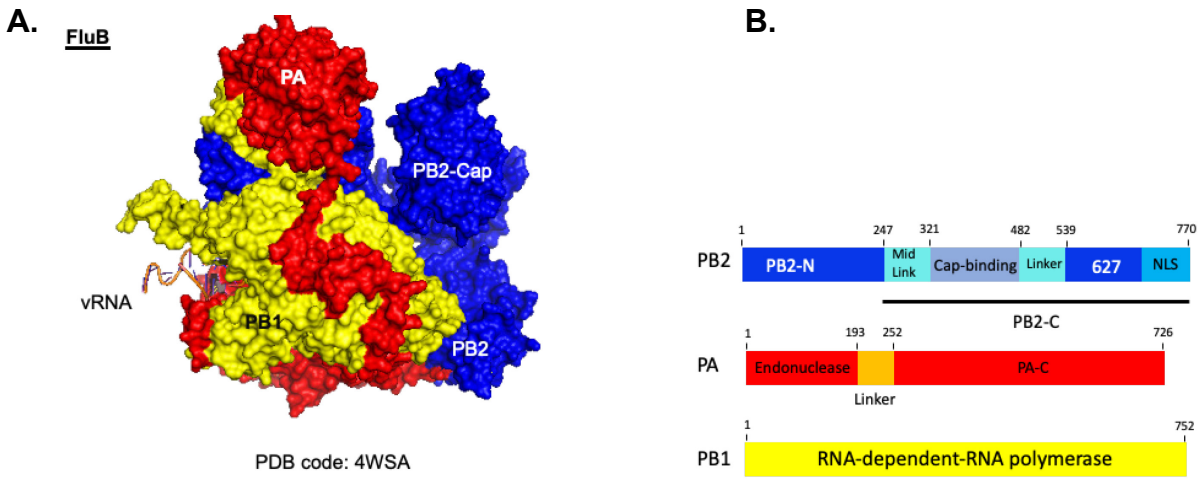

Figure 1.2: The Surface Diagram of Influenza B RdRp. The diagram shows the heterotrimeric FluB polymerase and how they link together. PDB Code: 4WSA. Figure is adapted from Reich et al, 2014 [33].

1.2.3 Viral Assembly and Virion Release

The newly synthesized RNAs within the cytoplasm need to be transported back to the nucleus for vRNP formation. Then, once again, they are transferred back to the cytoplasm where Endoplasmic Reticulum (ER) does the post-translational modification such as glycosylation. After that, the vRNPs are transferred to the cell surface using microtubule organizing centers (mTOCS). The conjoining of the HA and NA with the lipid bilayer membrane of the host cell starts the assembly process of the virions [34]. To form a complete virion, eight segments of the genome, which is in the form of the vRNP, should incorporate; this is mediated by segment-specific packaging signals. After the formation of the virion, liberty is another challenge on the way. NA protein cleaves the sialic acid on the surface of the host cell, and as a result, virions release from the cell as well as prevent virion clumping [35].

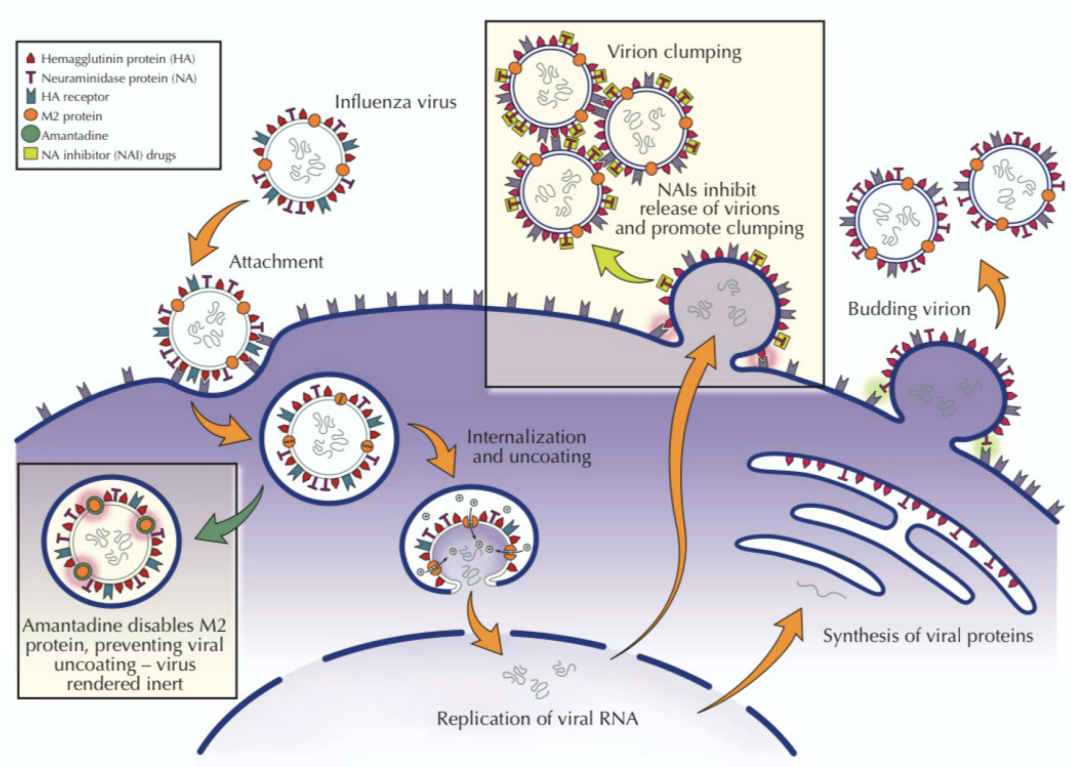

Figure 1.3: The Influenza A life cycle. The figure shows the steps in the viral entry, un-coating, replication and release of the newly formed virion. It also shows the target for two classes (M2-ion channels and NA inhibitors) of approved drugs. This figure is adapted from Shi et al, 2014 [26].

1.3 Influenza Vaccine

As discussed earlier in section 1, influenza virus infection imposes a high financial burden every year; therefore, having a prophylactic agent is crucial for society. Influenza vaccines are an effective way to reduce the mortality and morbidity related to influenza infection [37]. However, due to the highly variable nature of the virus, vaccines need to be updated annually; WHO maintains yearly global surveillance to predict the possible circulating strains of the virus for the following flu season [38],[39]. Producing enough doses of the vaccine takes about six months

each year. There are two different approved types of influenza vaccines: inactivated vaccines and Live Attenuated Vaccines (LAIV) [40]. Inactivated Vaccines are the whole virus inactivated and fragmented or purified antigens. Whereas in LAIV, attenuated master donor virus is used and designed to activate the cell response by intranasal administration [41]–[43].

1.4 Influenza Antivirals

Although influenza vaccines are available to prevent viral infections, it is unlikely to protect humans in case of the emergence of the newly evolved virus. Therefore, the development of antivirals for treatment during the possible pandemics plays a vital role.

So far, three classes of antivirals are developed to target the influenza virus, and they include: 1) M2 ion-channel inhibitors; 2) Neuraminidase inhibitors (NAIs); and 3) RdRp inhibitors.

1.4.1 M2-Ion Channel Inhibitors

The first class is M2 ion channel inhibitors: Amantadine (commercial name: Symmetrel) and its analogue, Rimantadine (commercial name: Flumadine) are examples of this class. They are the first approved antiviral to combat influenza infection [44]. As discussed in section 1.2.4, the M2 proteins are located within the lipid bilayer, and through them, hydrogen ion flows into the cell and results in the degradation of matrix protein 1 (M1), and uncoating and release of the vRNP into the cytoplasm (Figure 1.3) [45]. Since influenza B lacks the M2- ion channel, these drugs are only effective against influenza A [46], [47]. However, due to the high rate of resistance to this class, the Center for Disease Control and Prevention (CDC) strongly advises against prescribing them [48].

1.4.2 Neuraminidase Inhibitors (NAIs)

From 2010 to 2018, neuraminidase inhibitors are the only class of inhibitors that are recommended for the management of influenza A and B infection [49]. Oseltamivir, with the commercial name of Tamiflu, and Zanamivir, with the commercial name of Relenza, are the examples of this class of inhibitors. Neuraminidase is a surface protein that has a significant role in releasing the viral progeny from the host cell by cleaving the sialic acid. Due to the highly conservative nature of the active sites of an enzyme, the drugs can be designed in such a way that they can compete with the natural substrate of the NA—inhibiting the Neuraminidase results in failing to release the newly formed virus and forms clumps of the viruses due to attachments of Neuraminidase from one virion attached to the other one. Developing resistance is relevant to the mutations that can change the shape of the NA active site so that the drug-binding affinity decreases. The NA resistant strains that have been isolated emphasizes on the emergence of the new class of inhibitors that can inhibit influenza viruses regardless of the types and strains of the virus and lower chance of developing resistance [36], [50].

1.4.3 RdRp Inhibitors

RdRp inhibitors represent the third class of inhibitors. RdRp is highly conserved among all types of influenza A, B, and C. Inhibiting RdRp directly decreases the viral replication and transcription, as influenza RdRp possesses three different subunits that each can be targeted [50]–[53].

1.4.3.1 Favipiravir

Favipiravir (T-705) targets the PB1 subunit of the RdRp of all types of influenza virus. Favipiravir is a prodrug which is further phosphorylated by cellular enzymes and converted to the active form Favipiravir- ribofuranosyl 5'-triphosphate (F-RTP) [55]–[58]. The active triphosphate form is recognized as a purine analogue by RdRp. It was shown to be incorporated preferentially as adenosine and less as guanosine. Following its incorporation, the compound can terminate or inhibit chain elongation. Also, favipiravir can cause lethal mutagenesis by increasing G to A and C to U mutation and forming nonviable virions. Favipiravir is a broad-spectrum antiviral shown to be effective against several other RNA viruses. It is a weak substrate for human RNA polymerases that provides a certain degree of selectivity.

In 2018 Goldhill et al. described the PB1-K229R mutation in A/England/ 195/2009 (H1N1) [59]. The mutation decreases susceptibility to Favipiravir. However, this mutation is also associated with a diminution in viral replication fitness. The additional P653L mutation in the PA subunit can compensate for this deficit [59], [60].

1.4.3.2 Pimodivir

Pimodivir targets the PB2 subunit of influenza A RdRp that contains the cap-binding domain. This drug mimics the structure of the mRNA cap; therefore, it inhibits mRNA binding, which in turn affects the cap-snatching process [60]. Although Pimodivir efficiently inhibits the PB2 cap-binding process in influenza A, it is inefficient against influenza B. This is due to four reason: 1) Some of the crucial amino acids for inhibitor binding are different in the PB2 binding site of the influenza

A versus influenza B; 2) Some of the amino acids present in the cap-binding site of the influenza B sterically block Pimodivir; 3) Cap-binding affinity of the FluB is weaker comparing to FluA; and 4) Flu A RdRp binds specifically to the m7 G cap structure; however, FluB RdRp binds to the unmethylated capped mRNA [59]. Resistance to the Pimodivir has emerged during the *in vitro* passaging of the influenza A virus, and six different amino acid substitutions were shown to decrease drug susceptibility [59], [60].

1.4.3.3 Baloxavir Marboxil

Baloxavir Marboxil is a PA domain inhibitor that was approved in February 2018 in Japan and later in the US for the treatment of FluA and B infection. Within the human intestine, liver and blood esterase immediately breaks Baloxavir Marboxil to its active form, Baloxavir acid [60]. It is an endonuclease inhibitor that prevents cleavage of the bound mRNA in the cap-snatching process [63]. Inhibitors of the Human Immunodeficiency Virus (HIV) integrase show a similar mode of drug binding [64]. Like HIV integrase, the PA subunit uses divalent metal ion as a cofactor for endonuclease activity and Baloxavir acid binds to the divalent metal ion in the active sites of the PA subunit [65],[59].

The drug is shown to be highly efficient in inhibiting PA endonuclease activity. However, the I38T mutation in PA domain shows 22 to 41 decrease in viral susceptibility to influenza A [66].

1.4.4 Objective

The limitations of available antiviral drugs for the treatment of influenza infection is a problem that can potentially be addressed by combining different classes of RdRp inhibitors. Here we used a biochemical approach to study the selectivity of approved polymerase and endonuclease inhibitors. Combinations of these two classes of drugs could pave the way for the development of more effective therapies.

Chapter 2. Expression and Purification of FluB RdRp

2.1 Expression of the Recombinant RdRp

The Influenza B polymerase complex (PA/PB1/PB2) (Influenza B/Memphis/13/03) was expressed as previously described by Reich, et al. 2014 [67] and in our laboratory [1]. Genes coding for PA, PB1 and PB2 subunits as well as the gene coding for Tobacco Etch Virus (TEV) protease are inserted into p-FastBac plasmid downstream of the Baculovirus polyhedrin promoter. This gene cassette is flanked by Tn7 transposable elements (Figure 2.1). The resulting p-FastBac/TEV-PA-PB1-PB2 gene cassette is then transformed into DH10 E. coli. DH10 E.Coli contains Tn7 transposase expression plasmid and a recombinant Baculovirus genome (bacmid) that can be propagated in both E.Coli and insect cells. Bacmid contains (1) a gene coding for the Yellow fluorescent protein, which is under the control of the polyhedrin promoter, and (2) LacZα subunit gene which also contains Tn7 attachment site. Upon transformation of p-FastBac/TEV-PA-PB1-PB2 into DH10 E.coli, the endogenously expressed Tn7 transposase mediates insertion of TEV-PA-PB1-PB2 gene cassette into Tn7 attachment site within LacZα subunit gene, which in turn disrupts the LacZα subunit gene sequence and allows for blue/white screening of the E.coli colonies: E.coli containing bacmid with successfully integrated TEV-PA-PB1-PB2 gene cassette will appear white on the X-gal containing medium. The bacmid/TEV-PA-PB1-PB2 is then propagated and purified from DH10 E.Coli. Note that this bacmid/TEV-PA-PB1-PB2 contains two polyhedrin promoters: one upstream of TEV-PA-PB1-PB2 gene cassette, and a second one upstream of YFP gene (Figure 2.2).

Purified bacmid/TEV-PA-PB1-PB2 is transfected into Sf.9 insect cells to generate and amplify infectious baculovirus. Upon infection of Sf.9 with recombinant baculovirus the TEV-PA-PB1-PB2

genes are expressed as a polyprotein, which is then cleaved by TEV protease at its specific cleavage sites engineered between the individual components of the polyprotein. Expression of the YFP from the second polyhedrin promoter allows to monitor recombinant baculovirus life cycle within insect cells using fluorescent microscope. Note that the YFP fluorescence is only indicative of the successful infection of insect cells with the recombinant baculovirus; it provides no information on the expression levels of the TEV-PA-PB1-PB2 polyprotein. Once cleaved from the polyprotein, the PA, PB1, and PB2 from a hetero-trimeric complex which is purified from insect cells using Strep-Tactin affinity chromatography mediated by the Strep-tag located on the C-terminus of the PB2 subunit. The hetero-trimeric complex also contains a histidine tag on the N-terminus of the PA subunit which can also be used for PA/PB1/PB2 complex purification using the Ni-NTA affinity chromatography (Figure 2.1).

2.2 Monitoring the Expression

We monitored the expression of the RdRp complex by measuring cell density for four days post-infection and compared it with non-infected cells. The non-infected cells show a gradual increase in cell density, whereas density remains constant for infected cells. This suggests that the Baculovirus highjacks the cell machinery to produce RdRp of influenza B polymerase.

The Baculovirus expression cassette also carries a gene for the production of Yellow Fluorescent Protein (YFP) which co-expresses with our protein of interest. YFP is used as an indicator for the relative production of RdRp of Influenza B. To monitor the RdRp complex of influenza B, we measured the Relative Fluorescence Unit (RFU) emitted by YFP. The plotted RFU graph for infected and non-infected cells suggests that the production of RdRp of Influenza B substantially

increases after day two, whereas non-infected cells do not produce any YFP. To confirm the fluorescent production, we used Fluorescent microscopy. Pictures taken 60 hours post-infection, approved the YFP production in infected cells; however, non-infected cells do not show the production of YFP.

2.3 Purification of the Heterotrimeric RdRp Complex

After expressing the FluB polymerase heterotrimeric complex (PA, PB1, PB2) using Sf9 cells, we used Strep-Tactin Affinity Chromatography to purify the protein. We then confirmed the presence of the complex using Mass Spectrometry (MS) Analysis (Dr. Jack Moore, Alberta Proteomics and Mass Spectrometry). Elutions collected from the Strep-Tactin column ran in an 8% SDS-PAGE gel. MW (Molecular Weight) in Lane 1 represents a protein ladder. E1 to E5 (lane2-6) represents the elutions 1 to 5. To assess the purity of the enzyme preparation, we used elution number 3 as an example. In lane E3, we observe the major band corresponding to the FluB enzyme. We also observe a minor band illustrating an impurity present in the enzyme preparation. To assess the ratio of protein of interest to the sample's impurity, we loaded 20 times less of the enzyme preparation in lane E3-20x than in lane E3. Since we still observe a band corresponding to the protein of interest while no impurities can be seen, we concluded that there should be ~20 times more of the protein of interest than impurities in the preparation, which corresponds to ~95% pure protein (95%/5%=19, or ~20 fold ratio of protein of interest to the impurities).I used Strep-Tactin affinity chromatography to purify the protein, and W20 represents the washing of the Strep-Tactin column after 20 CV. The W20 suggests that we did not lose the protein of interest during washing steps.

The protein has an absorbance at 280nm. We pooled all the elutions together and measured absorbance at 280nm using nanodrop (Figure 2.3- B). Low absorbance at 280nm is expected (black line diagram) for the protein diluted at this time. We then used a 30kDa concentrator and measured the 280nm (red dotted diagram). The sharp peak suggests that we successfully concentrated our protein. To store the protein prep, we needed to add 45% glycerol (blue dashed diagram), and as a result, the absorbance decreased by approximately half.

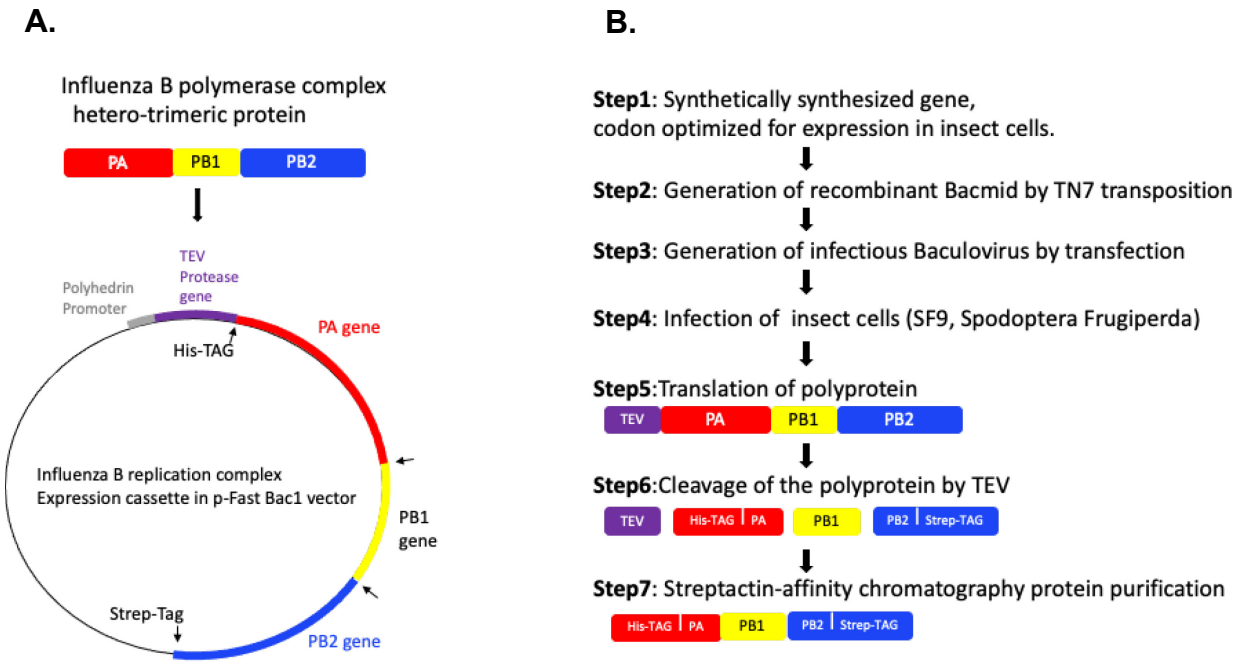

Figure 2.1: Expression of recombinant FluB polymerase complex (PA/PB1/PB2). (A) Schematic diagram of the influenza B polymerase complex expression cassette. The influenza polymerase is expressed as a polyprotein consisting of TEV (Tobacco Etch Virus) protease, PA, PB1 and PB2 with a TEV cleavage site (arrow) between each subunit. This TEV cleavage site facilitates the cleavage of the polyprotein into the individual components PA, PB1, and PB2. (B) Schematic detailing the generation recombinant Baculovirus and the expression/purification of the influenza B polymerase complex [67].

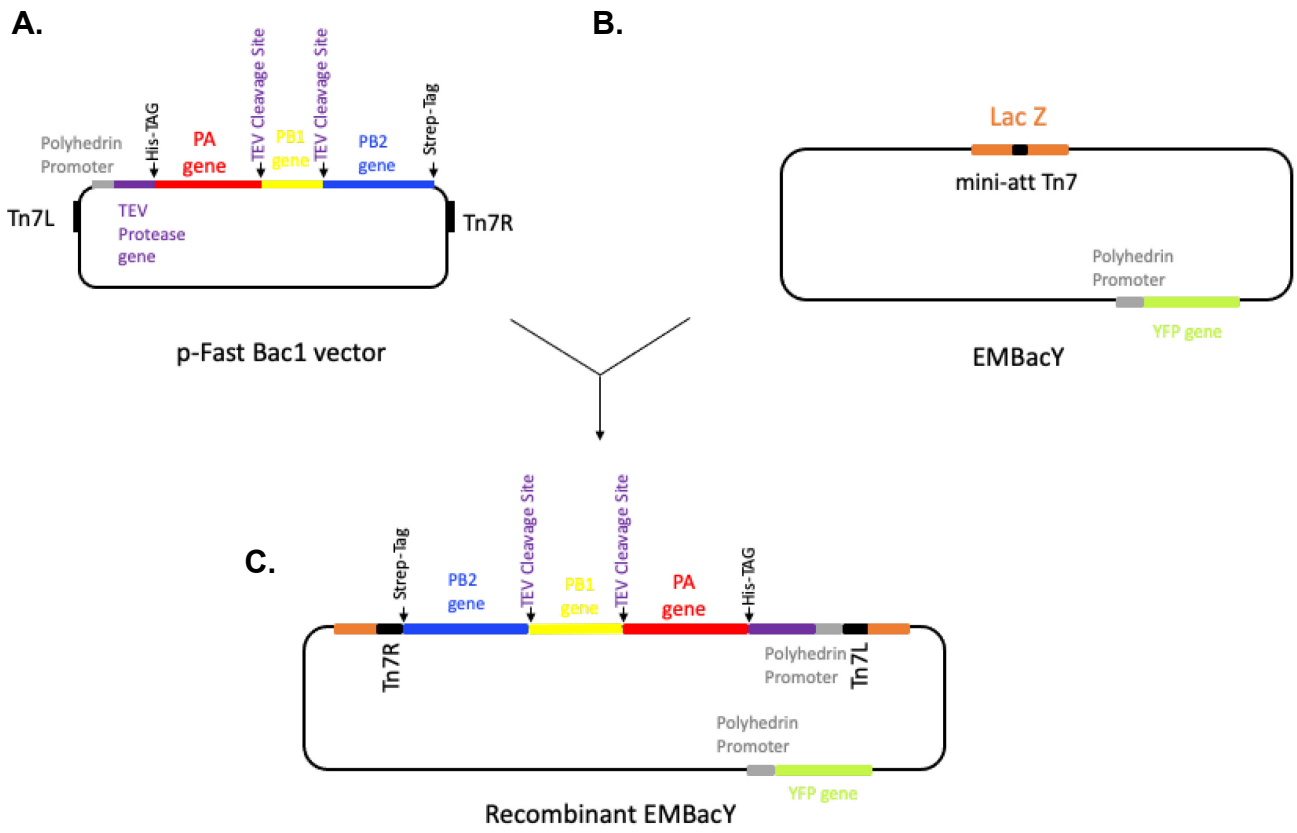

Figure 2.2: Transposition of the p-Fast Bac1 into the EMBacY expression plasmid. (A) Schematic diagram of the influenza B polymerase complex expression cassette flanked by transposable elements. (B) Schematic diagram details the EMBacY plasmid, the YFP gene's position, and transposition site for transposable elements within LacZ. (C) The recombinant EMBacY is the expression cassette which contains the RdRp of Influenza B polyprotein and co-expressed protein of interest and YFP [68].

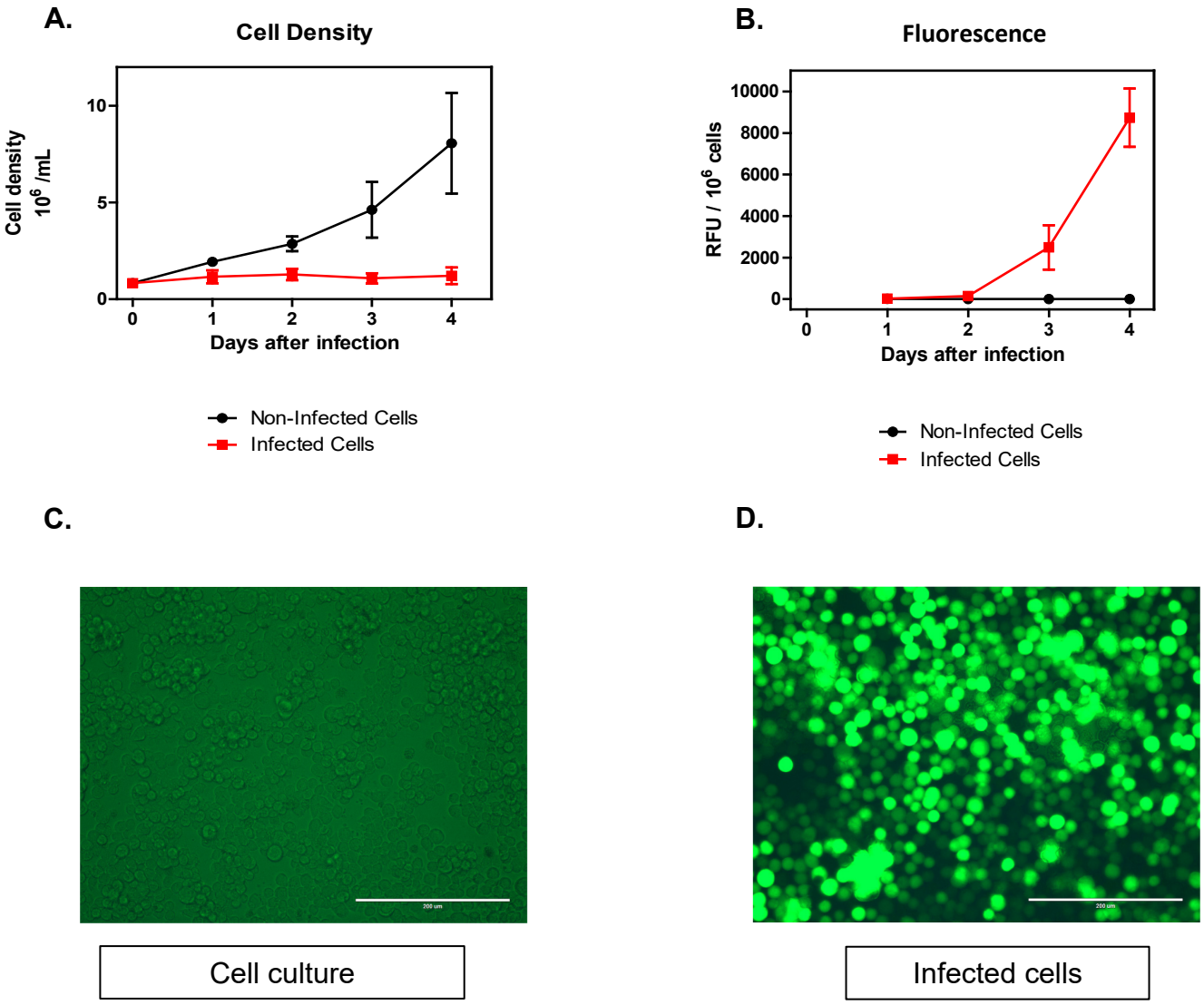

Figure 2.3: Monitoring expression of FluB polymerase complex. (A) Cell density of Baculovirus infected and non-infected cell cultures after four days. (B) RFU measured for four consecutive days in infected and non-infected cells. (C) Fluorescence microscopy of infected cells at 60 hours post infection. (D) Fluorescence microscopy of cell culture at 60 hours post passaging. Cells infected with recombinant Baculovirus appear green due to YFP production.

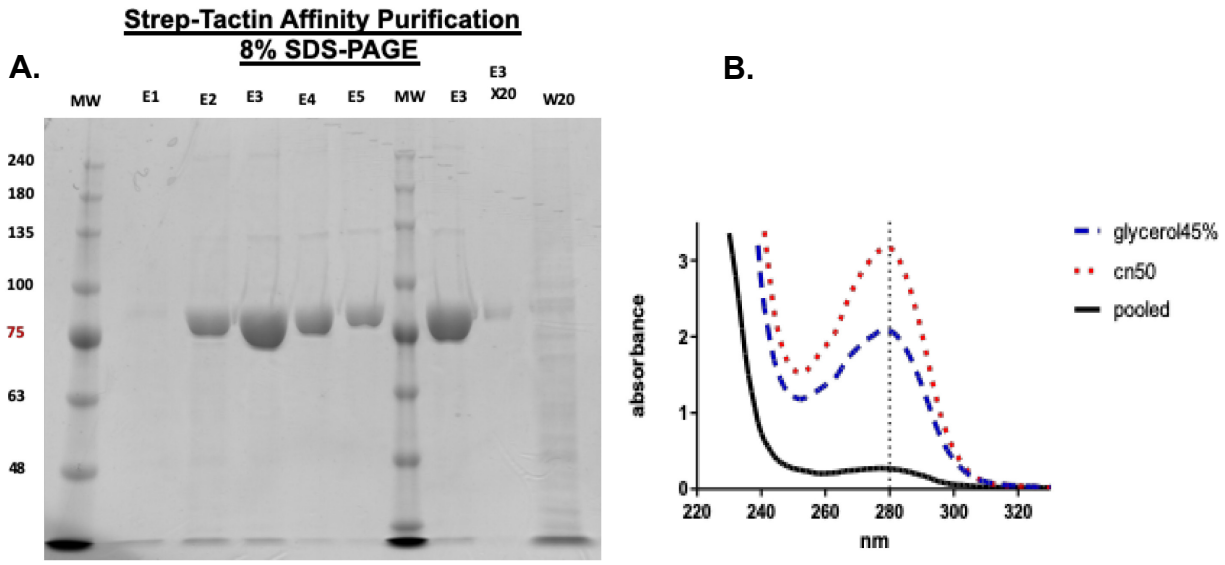

Figure 2.4: Purification of the FluB polymerase complex using affinity chromatography. (A) Elutions of the purified polymerase complex were resolved on an 8% SDS-PAGE gel and stained with Coomassie Brilliant Blue G250. MW represents the migration of a commercially available molecular weights ladder. (B) Absorbance at 280nm for unconcentrated pooled elutions (black line diagram), the elutions after concentration of a 50 kDa Millipore concentrator (red dotted diagram) and the final protein preparation after additions of 45% glycerol for storage at -20˚C (blue dashed line diagram).

Chapter 3. Inhibition of RdRp by Nucleotide Analogues

3.1.1 FluB RdRp Assay

To assess the enzymatic activity of the expressed recombinant FluB RdRp, we established a primer/template-based system [1]. The template is 11 nucleotides long and complementary to four nucleotides primer and phosphorylated at the 5'-end. The primer/template system is designed to allow the incorporation of radio-labelled nucleotide as the first nucleotide incorporation site.

Four nucleotides primer and eleven nucleotides template are radio-labelled as a marker for distinguishing the pattern of migration due to primer extension and full-length product. Lane 1 shows that during RNA synthesis, the first nucleotide incorporates at position five (+1) is the radiolabeled GTP. In lane 2, the ATP incorporates at positions 7 and 8, and lane 3 shows that if ATP and CTP are present in the reaction, the mixture yields to the formation of full-length products. Lane 4 shows that the FluB RdRp recognizes ara-CTP, a nucleoside analogue and incorporates it at position 8. The ara-CTP acts as a chain terminator, and RNA synthesis stop at eight nucleotides. Lane 4 suggests that the products contain ara-CTP migrate differently than natural CTP. Having this assay established, we were confident to use this system as a reliable assay for further analyses.

3.1.2 Nucleotide analogues screening

Using the commercially available drugs to inhibit the viral infection is an efficient way to control the viral infection. Therefore, with the established primer/template-based system (Figure 3.1) which represents the RNA synthesis elongation, I screened a library of CTP analogues for potential nucleotide analogue inhibitors of the FluB RdRp. We checked the inhibitory effect of

the commercially available CTP nucleoside analogues which incorporates at position eight and terminate RNA synthesis. To test the nucleoside, we used the established 4-nt primer and 11-nt template which allows the incorporation of radio-labeled GTP at position 5 and ATP at position 6 and 7. If the reaction mixture contains natural CTP, it incorporates at position 8 and yields to full length product which is 11 nucleotide long RNA.

In lane 1 only ATP presents in the reaction mixture with final concertation of 1 µM which yields to 7 nucleotide products. As it is shown in lane 2 adding CTP to the growing RNA strand results in production of full-length RNA (11 nucleotide). This lane is a control, which shows how the system works in the absence of the possible CTP analogue inhibitor. Lane 3 shows FluB RdRp that recognizes araCTP and incorporates it against position 8; and because no RNA synthesis is observed after that, araCTP shows inhibition pattern in this set up. In lane 4, the products at position 8 and formation of full-length product suggest that 2'dCTP have partial inhibitory effect on influenza B polymerase, whereas in lane 5, 8, and 9, the relative nucleoside analogues show inhibitory pattern with no further RNA extension after position 8. However, nucleoside analogues used at lane 6, 7, 10, 11, and 12, shows no inhibitory effect and the formation of full-length product is evident. The final concentration of nucleoside analogues is 100 µM versus 1 µM of the natural nucleotide.

3.1.3 Selectivity of the araCTP

The previously shown screening of commercially available nucleoside analogues showed that araCTP is a bona fide inhibitor of FluB RdRp. Using a model primer/template, we designed the experiment for the incorporation of α ^{32}P-GTP at position five that allows the detection of the

reaction products. Product 7 illustrates the 4-nt primers that were extended by three nucleotides such that in the absence of CTP the enzyme is poised for incorporation of CTP opposite G in the template (lane 0). Supplementing the reaction mixtures with increasing concentrations of CTP allows the enzyme to utilize CTP (or ara-CTP) as substrate for nucleotide incorporation across G in the template.

Addition of increasing concentrations of ara-CTP, which acts as an immediate chain-terminator here, results in disappearance of signal corresponding to product 7 and appearance product 8 which corresponds to nucleotide incorporation opposite template G. The ratio of signal intensity of product 8 to the total signal in product 7 and 8 is indicative of the fraction of the 7-nucleotide primers that were extended by one nucleotide (product 8 fraction) and illustrates the concentration dependence of ara-CTP utilization as substrate for nucleotide incorporation. Plotting the product 8 fraction as a function of ara-CTP concentration and fitting the data points to Michaelis-Menten equation allows the calculation of the maximal velocity of ara-CTP incorporation (Vmax) and concentration of the ara-CTP substrate at which the velocity of ara-CTP incorporation is half-maximal (Km). Vmax and Km are also referred to as Michaelis-Menten parameters for nucleotide incorporation.

Note that in case of CTP incorporation (Fig. 3.5, left panel) the RNA synthesis doesn't stop at position 8 because the reaction mixtures also contain ATP for incorporation past G in the template, hence, the RNA synthesis proceeds till the end of the RNA template to form products 9, 10, and 11. Therefore, in order to determine the Michaelis-Menten parameters of CTP utilization as a substrate for nucleotide incorporation opposite G in the template we determined the ratio of the sum of signal intensities of products 8 through 11 to the sum of the signal

intensities of products 7 through 11. Plotting the product 8-through-11 fraction as a function of CTP concentration and fitting the data points to Michaelis-Menten equation allows the calculation of Vmax and Km for CTP utilization as a substrate for nucleotide incorporation.

Selectivity is defined as the ratio of V_{max}/K_m of a natural nucleotide over V_{max}/K_m of a nucleoside analogue that obtains from the Michaelis-Menton equation. V_{max} represents the maximum velocity of the reaction, and K_m is the substrate concentration when the velocity of the reaction is half of the maximum value. The selectivity values closer to 1 suggest that nucleoside analogues incorporate as efficiently as a natural nucleotide.

To obtain the selectivity value for araCTP, In Figure-3.5, we quantified the intensity of each band as a representative of single nucleotide incorporation by FluB RdRp with respect to the template. Then we fit the 12 data point values in the Michaels-Menton equation and plot it with Graphpad prism (Figure 3.5-A). The obtained V_{max} values for CTP and araCTP were 0.88 and 0.77, respectively, and K_m values were 0.048 and 0.075 µM (Figure 3.5-B). We used the equation in Figure 3.5-C to calculate the selectivity of the araCTP versus natural CTP, and the result is 23. It means our enzyme incorporates natural CTP 23 times better than araCTP. This suggest that araCTP might be an effective inhibitor of FluB RdRp, considering that a single incorporation of the nucleotide analogue causes chain-termination [1].

3.1.4 Resistance to Favipiravir

T-705 (6- fluoro-3hydroxy-2-pyrazinecarboxamide), also known as Favipiravir, is a selective RdRp inhibitor that does not have a substantial effect on cellular RNA synthesis [55]. At first, it was shown to be effective against influenza virus infection; but later, it showed to be effective against

a broad spectrum of RNA viruses. It is a prodrug and needs phosphoribosylation to the active triphosphate form [60]. The drug is a purine analogue, and RdRp of influenza virus can utilize it mostly instead of GTP, and less ATP can cause lethal mutagenesis [58].

In 2018, Goldhill et al. found a double mutation that is associated with resistance to the Favipiravir in MDCK cells infected by Influenza A/England/195/2005. One mutation was found in the F motif of the PB1 subunit when Arginine (R) substitutes the Lysin (K) at position 229 (K229R). F motif is located in the palm and interacts and bind with incoming NTP triphosphate [68], [69]. The K229R mutation is associated with a viral fitness deficit. However, with the second mutation in the PA subunit where Leucine in position 653 substitutes Proline (P653L) polymerase can compensate for the viral fitness deficit. This is the first report of a mutation in influenza A that confers resistance to Favipiravir [59].

3.1.5 Sequence and Structural alignment at K229

According to the paper published by Goldhill et al., K229 in the F motif of RdRp of influenza A virus strains were conserved. Therefore, we used T-Coffee to align the PB1 subunit of different strains of influenza A, B and, C. We observed that the lysin in position 229 is conserved among all types and strains of influenza virus. Goldhill et al. also suggested that K229 plays a role in NTP binding during RNA synthesis (Figure 3.7-B) [59].

Other studies [56], [70] showed that structurally related RdRp enzymes show similar patterns of resistance. In 2014, Delang et al. showed that mutation of K291R within the F motif of the RdRp of Chikungunya virus confers resistance to Favipiravir [70]. In 2017, Abdelnabi et al. showed that mutation of K159R within the F motif of the RdRp of Coxsackievirus B3 confers resistance to

favipiravir as well [56]. Chikungunya and Coxsackievirus B3 (CVB3) are single-stranded positive-sense RNA viruses. Using Pymol, we aligned the structure of RdRp of CVB3 (PDB code: 3CDW) with the PB1 subunit of RdRp of FluB (PDB code: 4WSA). We observed that lysine at position 229 (K229) in the FluB-PB1 subunit aligns perfectly with lysin at position 159 (K159) in RdRp of CVB3. The alignment suggests that the K159 in CVB3 RdRp resembles the amino acid of K229 in FluB RdRp, and both are responsible for nucleotide incorporation during RNA synthesis. It also shows that in both negative and positive sense RNA viruses, substitution of K to R in these positions, confer resistance to Favipiravir.

3.1.6 Purification of the FluB PB1-K229R mutant RdRp Complex

We expressed and purified the FluB mutant PB1 K229R using the same protocol as the WT FluB RdRp complex [67]. Figure 3.8-A shows the migration pattern of WT and mutant enzymes on 8% SDS-PAGE gel. MW represents the Molecular Weight of each subunit (PA=91 kDa, PB1=86 kDa and, PB2=90 kDa). The bands migrate just over 75kDa Mw. FluB PB1-K229R does not migrate differently in comparison with the FluB WT polymerase complex.

The absorbance for WT and the mutant enzyme was measured at 280 nm. WT enzyme is represented by a black line graph, while PB1-K229R mutant is a red line graph (Figure 3.8-B). The sharp peak suggests that the concentration of our protein preparation was successful. Both enzyme preparations were concentered on 50 kDa Millipore concentrators and stored in 45% glycerol at -20 °C. Table (C) shows the absorbance at 280nm for WT of 2.57 and PB1-K229R RdRp of 2.75, which suggests that the concentration of both enzymes is almost similar.

3.1.7 PB1-K229R mutant Gel-based Assay

We expressed and purified the FluB RdRp mutant complex (PA/PB1-K229R/PB2, following an approach described by Reich et al. in 2014 and used to express and purify the WT RdRp of FluB [33], [1]. We tested the enzymatic activity of the FluB PB1-K229R and wild type enzyme side by side. The schematic reaction shows 14 nucleotide RNA substrate and four nucleotides 5'-P primer (Figure 3.10-A). In this experiment, we designed the substrate in such a way that allows α ^{32}P-GTP for the first nucleotide incorporation at position 5. Also, either natural ATP or ATP analogues incorporates at position 6.

In the established assay, we tested the inhibition of FluB WT and PB1-K229R mutant by Favipiravir (Figure 3.10-B). We titrated Favipiravir up to 100 µM in three-fold dilution. We then quantified each band as single nucleotide incorporation with respect to the RNA substrate and fitted the values in the Michaelis-Menton equation using Graphpad Prism and obtained V_{max} and K_m values. The error bars are based on the standard deviation of three independent experiments. Figure 3.10-C suggests that in the same assay condition, the FluB PB1-K229R incorporates Favipiravir almost half of the FluB WT.

3.1.8 PB1-K229R Resistance values

In the previous figure, we showed that the FluB PB1-K229R mutant incorporates Favipiravir with an efficiency of almost half in comparison with the WT enzyme. We chose two more nucleotide analogue, Ribavirin and araATP. Ribavirin shows structural similarities with Favipiravir. However, araATP is structurally different. We asked if PB1-K229R mutation confers resistance relative to the structure of the nucleotide analogue.

To test that, I titrated the mentioned nucleoside analogues up to 100 µM in 3-fold dilutions. I quantified gels and fitted them into the Michaelis-Menton equation, and K_m and V_{max} values were calculated. Efficiency is the efficiency of single nucleotide incorporation during RNA synthesis for the FluB enzymes, and it is calculated as the ratio of V_{max} to K_m. Selectivity is the ratio of V_{max}/K_m of ATP to V_{max}/K_m of inhibitor. Resistance is calculated as the ratio of the selectivity of the PB1-K229R mutant enzyme to the WT enzyme. The standard error (std.err) is associated with the fit. The WT enzyme incorporates ATP with an efficiency of 26 and incorporates Favipiravir, Ribavirin and araATP with an efficiency of 1, 0.3 and, 0.01, respectively. The nucleotide incorporation efficiency by PB1-K229R enzyme for ATP, Favipiravir, Ribavirin and, araATP is 34, 0.15, 0.07 and 0.18. Then the selectivity value calculated for Favipiravir by WT enzyme is 25. This means the WT enzyme incorporates natural nucleotide 25 times more efficiently than Favipiravir. However, the same value calculated for the PB1-K229R enzyme is 224. This leads to a resistance value of 9, which means that the PB1-K229R mutant enzyme incorporates Favipiravir 9 times less than the WT enzyme. Accordingly, the resistance value for Ribavirin is five and for araATP is 0.1. This data suggests that PB1-K229R incorporates Ribavirin 5 times less than the WT enzyme. However, the PB1-K229R mutant enzyme shows no resistance to araATP; perhaps our preliminary data shows that it incorporates araATP more efficiently than the WT enzyme. Overall, the data suggest that the mutation confer resistance in FluB RdRp, and it is related to the structure of the nucleoside analogues.

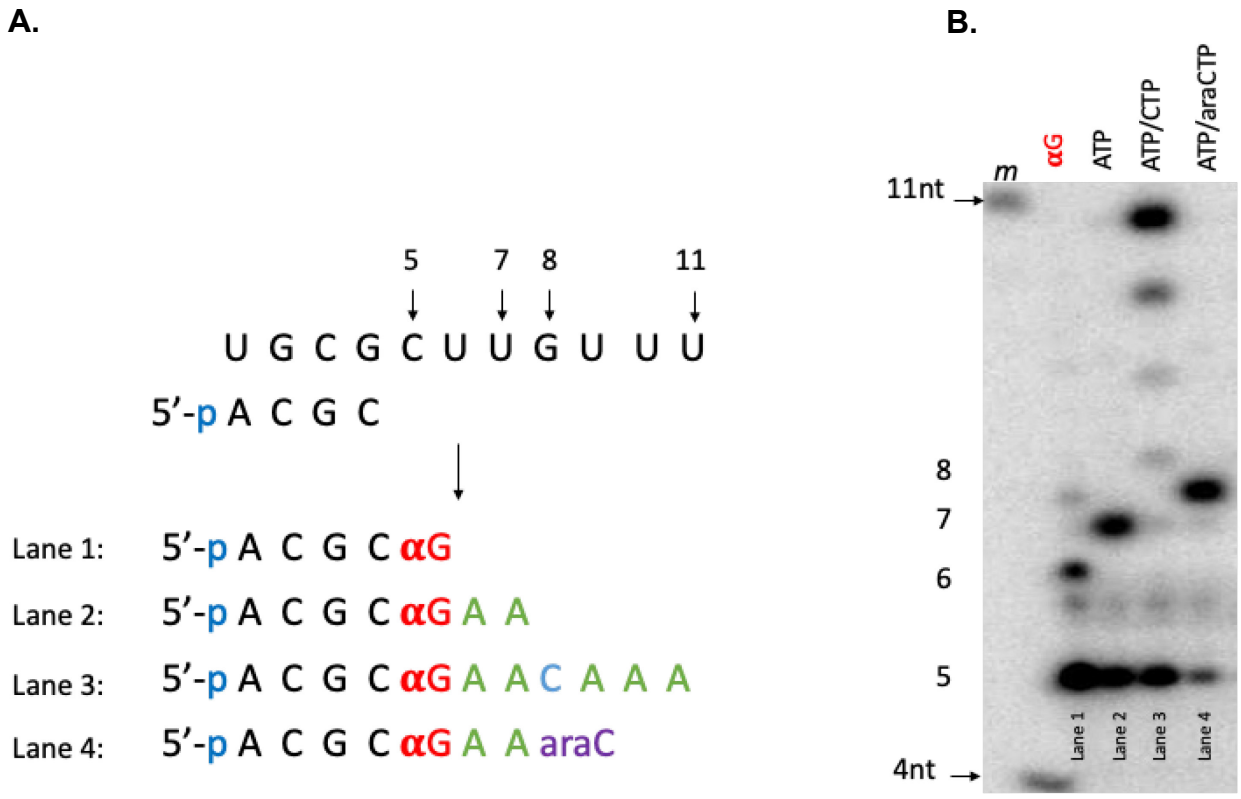

Figure 3.1: Assessment of limited RNA Synthesis by the FluB RdRp Complex. (A) The schematic reaction shows the addition of a natural nucleotide, which yield to primer extension and result in five, seven and eleven nucleotides products (lane 1 to 3). Additionally, ara-CTP, a nucleotide analogue (the structure shown in Figure 3.1.2), can be recognized by FluB polymerase and incorporates against eight position (lane4). (B) 15% denaturing PAGE shows the migration pattern of the RNA synthesis products.

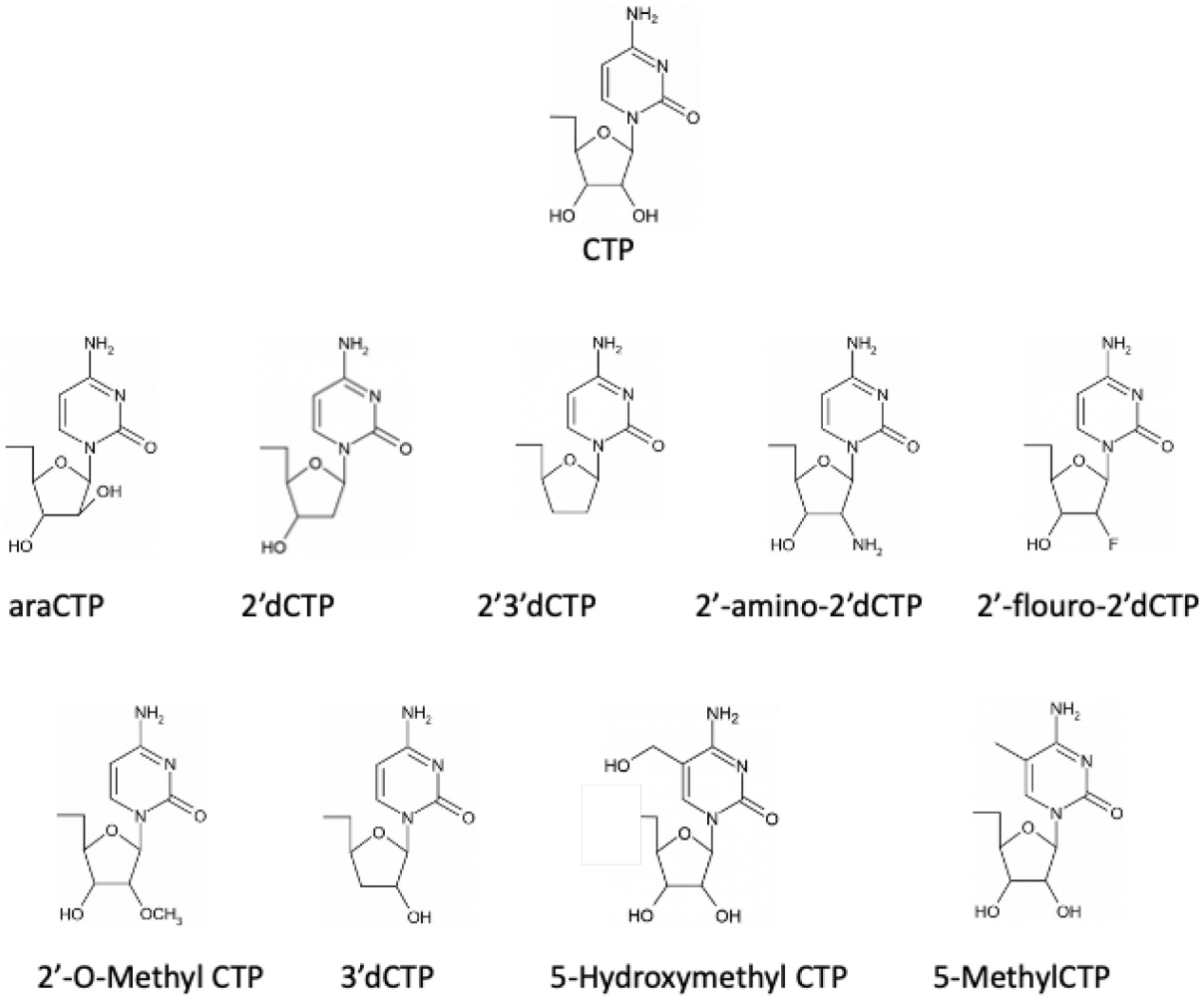

Figure 3.2: Chemical Structure of CTP analogues. Tested CTP analogues for screening possible inhibition of FluB RdRp.

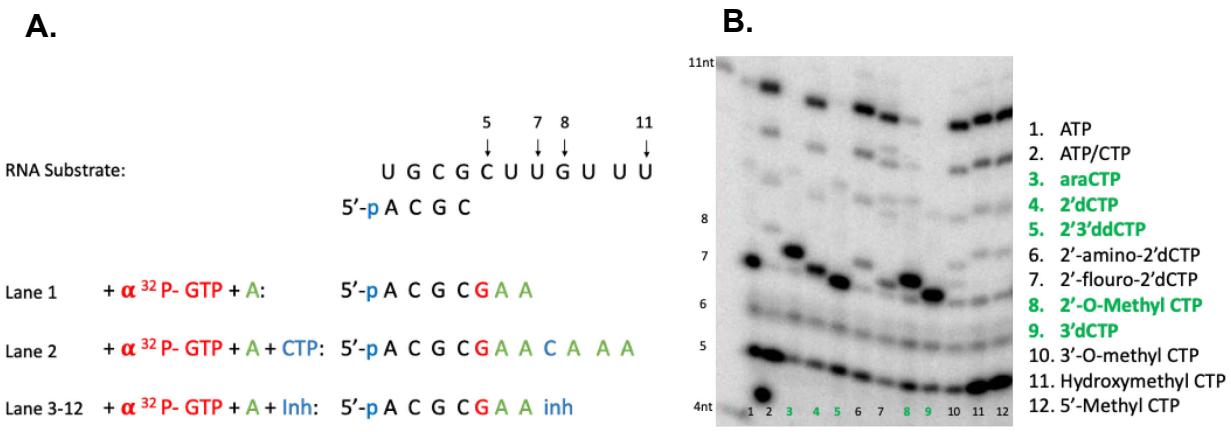

Figure 3.3: RNA Synthesis by Influenzas B Polymerase Complex in the presence of different nucleoside analogues. (A) The schematic shows the sequence of primer template that allows the first incorporation for radio-labeled nucleotide. Lane 1, ATP shows the migration pattern for 7 nt products. Lane 2 and 3-12 shows the expected products for natural nucleotide incorporation versus analogues with inhibitory effect. (B) Screening CTP analogues has been done using established primer-template system. The nucleoside analogues which show inhibitory pattern are colored in green.

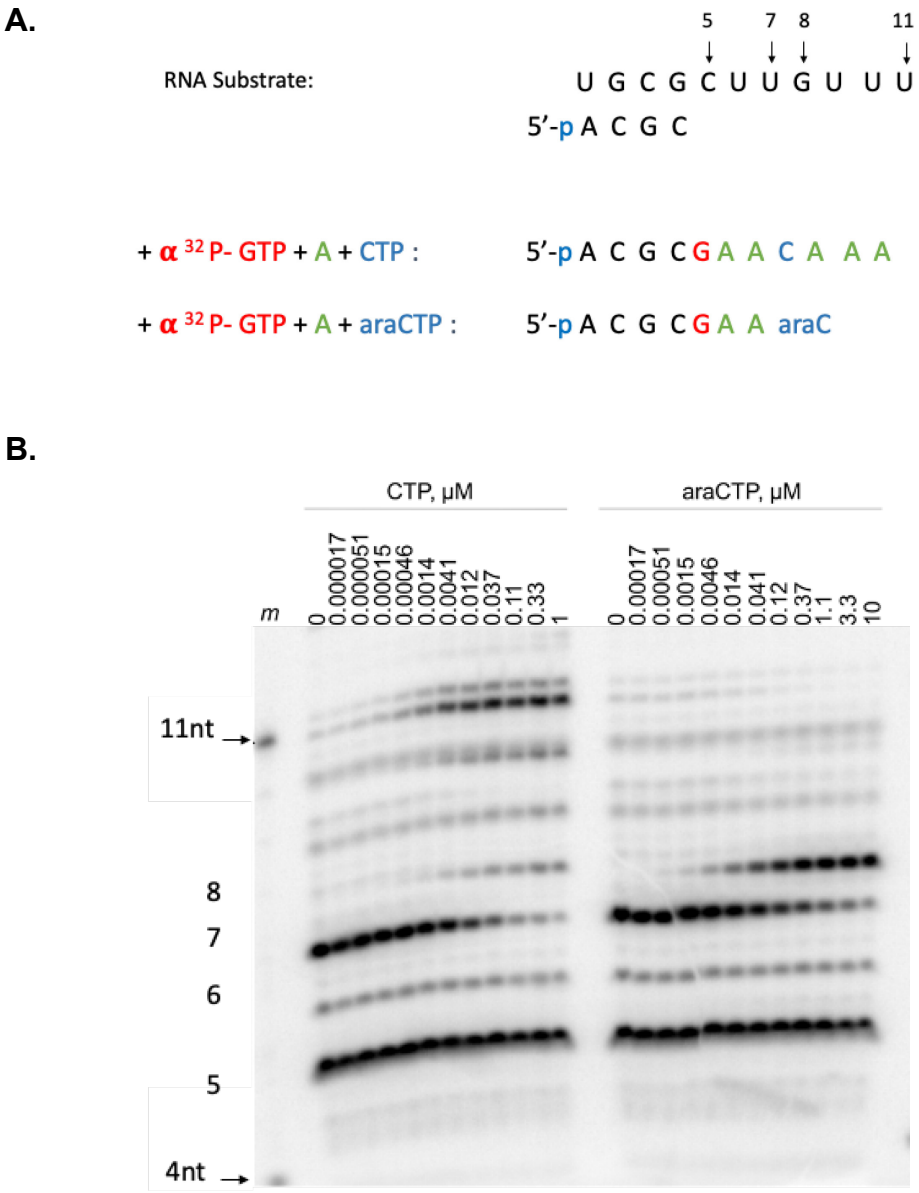

Figure 3.4: Efficiency of CTP and ara-CTP incorporation. (A) Schematic detailing the sequence of RNA template and primer used in this experiment. (B) 20% denaturing PAGE shows the migration pattern of increasing concentration of CTP and araCTP. Lane M indicates the migration pattern of the radio-labelled primer (4nt) and radio-labelled template (11nt), here used as molecular weight marker.

A.

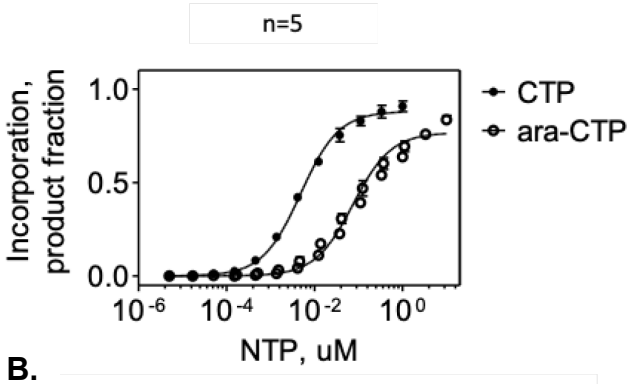

B.

Michaelis -Menton	CTP	araCTP
V_{max} (P.frac)	0.88	0.77
K_m (μM)	0.048	0.075

V_{max}: Maximum velocity of reaction

K_m: [Substrate] where v = 1/2 V_{max}

C.

$$Selectivity = \frac{CTP\ (V_{MAX} \div Km)}{araCTP\ (V_{MAX} \div Km)}$$

$$Selectivity = \frac{CTP\ (0.88/0.0048)}{araCTP\ (0.77/.0.075)}$$

$$Selectivity = 23$$

Figure 3.5: Data analysis of araCTP during RNA synthesis by FluB RdRp. (A) Fraction of 11 and 8 nucleotides product as a function of CTP and araCTP concentration, respectively. Error bars are based on the standard deviation of five independent experiments. (B) 12-data point values calculated by fitting the data shown in A to the Michaelis-Menton equation using Graphpad Prism. Product fraction (P. frac) is the fraction of the extended primer. (C) calculation of selectivity values for araCTP.

A.

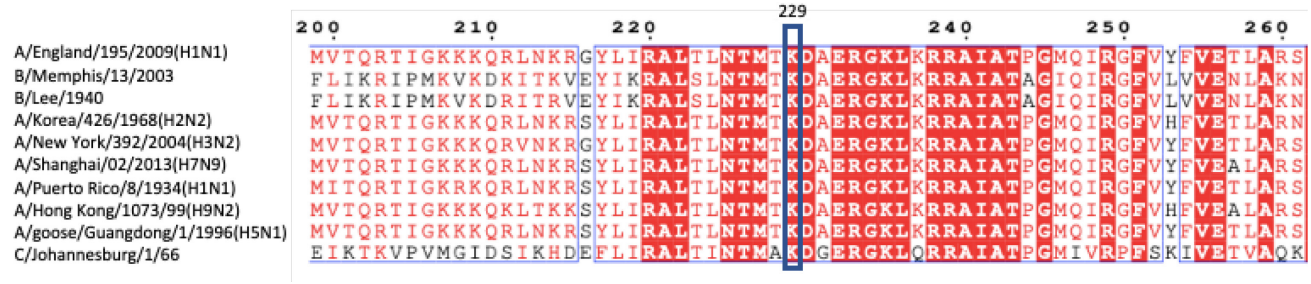

B.

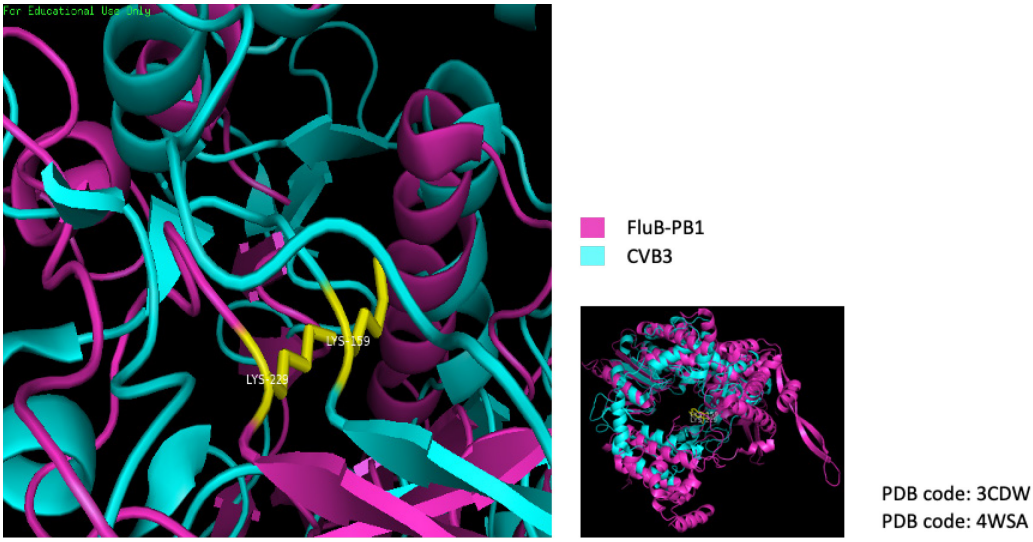

Figure 3.6: Sequence and structure alignments. (A) The sequence alignment (T-Coffee) of PB1 subunit of RdRp enzyme for different strains of influenza type A, B, and C. The alignment represents the conserved Lysine (K) at position 229 within PB1 motif F of all types and strains of the influenza virus. (B) Structural alignment of RdRp of coxsackievirus B3 (CVB3) (PDB code: 3CDW) and FluB (PDB code: 4WSA).

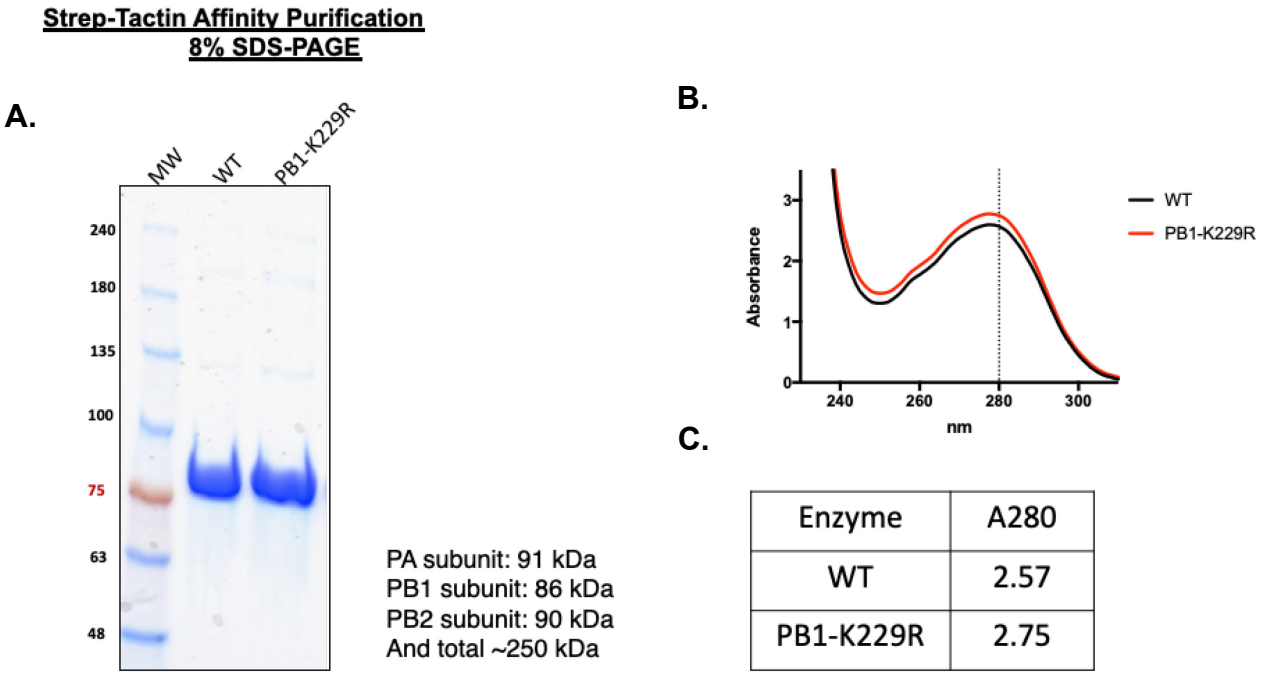

Enzyme	A280
WT	2.57
PB1-K229R	2.75

Figure 3.7: Purification of mutant FluB PA/PB1-K229R/PB2 complex. (A) Purified WT and PB1-K229R polymerase complex were resolved on 8% SDS-PAGE gel and stained with Coomassie Brilliant Blue G250. MW represents Molecular Weight. (B) the absorbance of WT and mutant FluB polymerase complex at 280nm. (C) The reads for WT and Mutant enzyme complex at 280 nm.

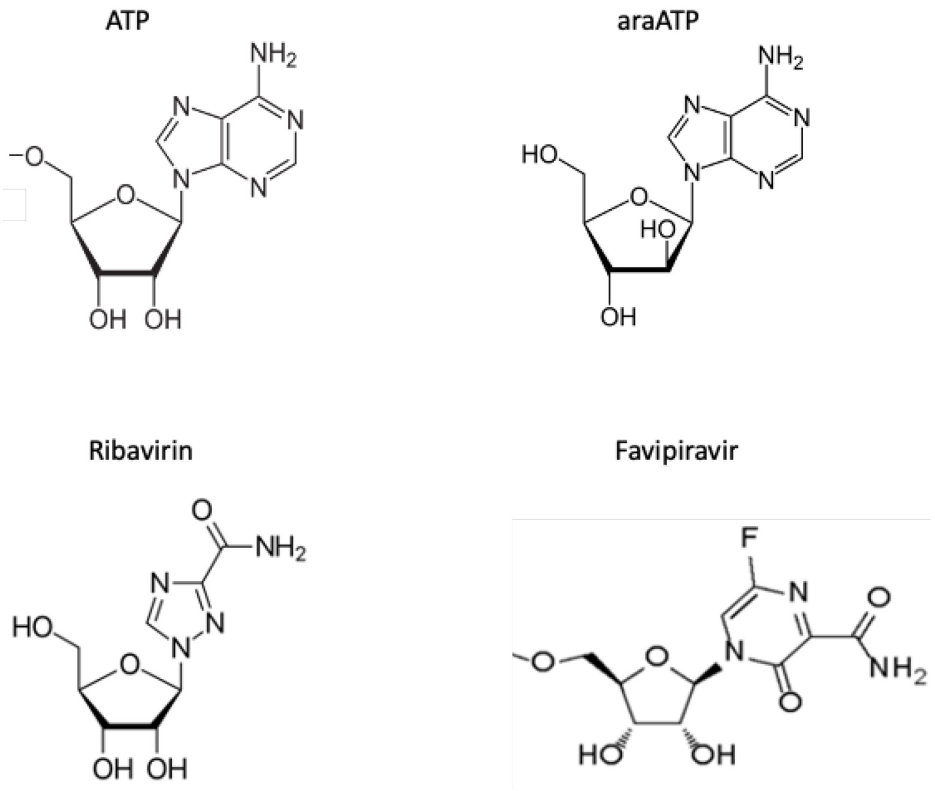

Figure 3.8. Chemical structure of the Adenosine nucleotide substrate analogues used in the study.

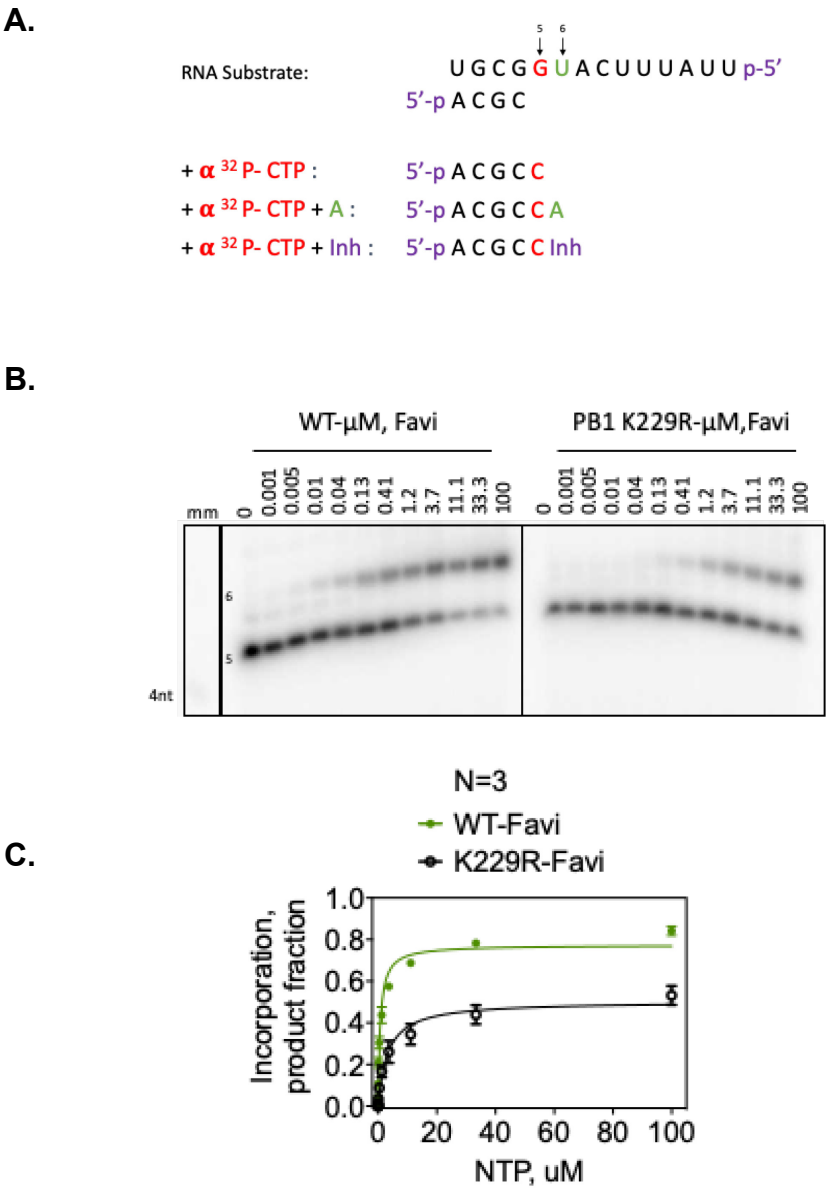

Figure 3.9: Patterns of Favipiravir Incorporation for WT and PB1-K229R FluB RdRp. (A) Schematics detailing the sequences of RNA substrate and primer used in this experiment. 5'P indicates 5' phosphorylation. (B) 15% of denaturing PAGE-gel shows the pattern of migration for Favipiravir by FluB WT and PB1-K229R mutant. "mm" represents the migration pattern of 4 nucleotides radiolabeled ACGC primer (C) Quantification of the data presented in B.

	WT					K229R			
	ATP n=3	Favipiravir n=3	Ribavirin n=3	araATP n=4		ATP n=3	Favipiravir n=3	Ribavirin n=3	araATP n=4
V_{max} (p.frac)	0.77	0.77	0.52	0.039		0.68	0.5	0.4	0.42
std.err	0.023	0.032	0.026	0.031		0.03	0.021	0.01	0.021
K_m (μM)	0.03	0.74	1.8	3.5		0.02	3.3	5.4	2.4
std.err	0.004	0.16	0.26	1.2		0.0041	0.58	0.54	0.54
V_{max}/K_m (Efficiency)	26	1	0.3	0.01		34	0.15	0.07	0.18
Selectivity		25	89	2303			224	459	194
Resistance							9	5	0.1

Table 3.1: Resistance values for Favipiravir, Ribavirin and araATP nucleotide analogues. The values obtained based on 12 data-point experiments, performed independently and at least three times (n=).

Chapter 4. Inhibition of RdRp by Metal Binder Compound

4.1 Chemical Structure of Baloxavir Acid

Baloxavir Acid (BXA) inhibits the endonuclease activity of Flu RdRp by binding to the catalytic divalent metal ions at the active site of PA. Lacbay et al. [71] have shown that pyrophosphate-like analogues can bind to the Polymerase and Ribonuclease H (RNase H) active sites of HIV-1 reverse transcriptase. Because influenza RdRp also possesses polymerase and nuclease active sites, we hypothesized that compounds with the ability to bind divalent metal ions may target both sites.

4.2 RdRp Activity in the Presence of Baloxavir Acid

To test the hypothesis, we titrated Baloxavir Acid (Figure 4.1) and tested it in Endonuclease and RdRp assay separately.

The symmetrical RNA substrate used in this assay is a 14 nucleotides RNA that the 3' end is complementary to each other. The system is designed in such a way that the first nucleotide that incorporates is a radiolabeled nucleotide which allows detection of the product of RNA synthesis. The reaction mixture contains a substrate, α ^{32}P- CTP, ATP to form 8 nucleotides products. The RNA synthesis starts with adding Mn^{2+}, and after 30 minutes, we added UTP and increasing the concentration of metal binder compounds. The reactions were then allowed to proceed for an additional 30 minutes and quenched. Inhibition was indicated by the lack of 9 nucleotide products. Conversely, if the metal binder compound did not have an inhibitory effect, we would see the 9 nucleotide products (Figure 4.2).

4.3 Endonuclease Assay

The endonuclease assay is designed in such a way that it contains an activating vRNA which is required for efficient endonuclease activity [72], [73]. The detection of the product is facilitated by a radio-labelled capped RNA substrate. The reaction comprises vRNA that increases concentration of the metal binder compounds and Mg^{2+}. The endonuclease reaction is initiated with substrate and stopped after 8 minutes. If the enzyme is inhibited by the metal chelating compound being tested, we would see no shorter product bands (12nt major product and 14 + 11nt minor products) than the substrate. If the RdRp of FluB is not inhibited, the endonuclease will cleave all the provided substrate, generating the shorter 14, 12, and 11 nucleotides products (Figure 4.3).

4.4 Inhibition Measurements with Baloxavir

We titrated the Baloxavir Acid up to 100 μM in RdRp assay and up to 10 μM in the Endonuclease assay (Figure 4.4 A-B). For the polymerase assay, we quantified each band as a representative of single nucleotide incorporation. Then, we calculated the fraction of 9 nucleotide products and calculated the IC_{50}. IC_{50} stands for the inhibitor's concentration at which enzyme activity is half of the activity in the absence of inhibitor. The quantified activity of the enzyme in the presence of an increasing inhibitor concentration is plotted versus inhibitor concentrations and fitted to the IC_{50} function using Prism software (Figure 4.4-C). However, the IC_{50} values in Endonuclease assay were obtained by the calculation of the fraction of the cleaved bands.

The reported IC_{50} values for Baloxavir are 13 and 0.0012 μM in RdRp and Endonuclease assay, respectively. The huge difference in IC_{50} concentration suggests that Baloxavir is a selective endonuclease inhibitor.

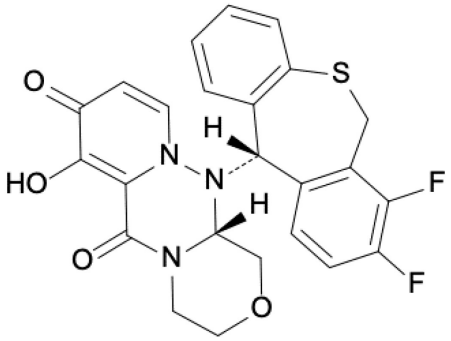

Baloxavir Acid

Figure 4.1: Baloxavir Acid structure. It is a divalent metal-ion chelating compound

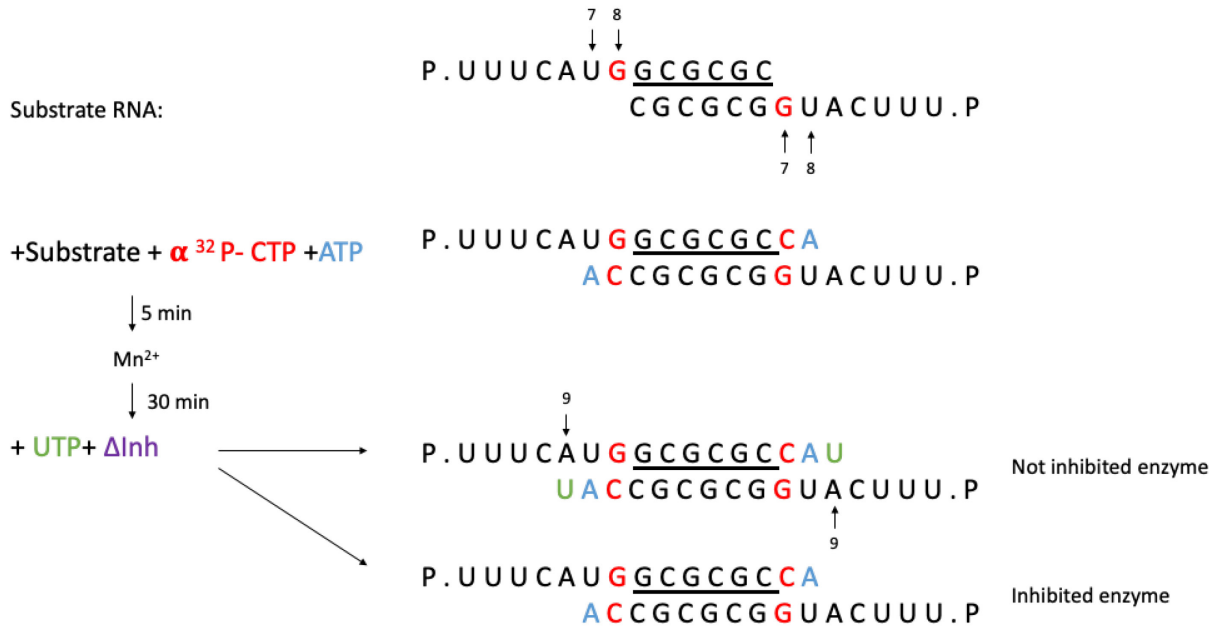

Figure 4.2: Polymerase Assay Reaction Schematic. Schematics detailing the symmetrical RNA substrate system, here utilized for compound screening.

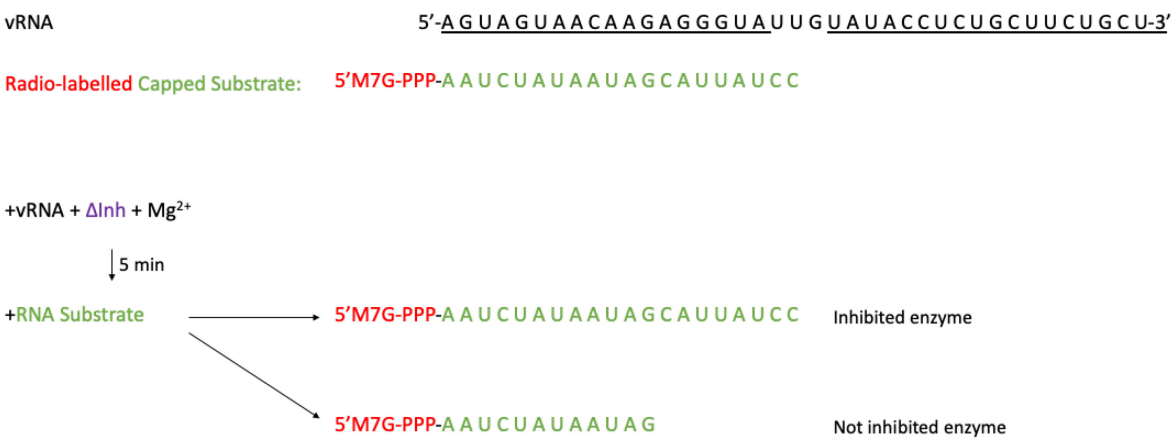

Figure 4.3: Endonuclease Assay Reaction Schematic. Schematic detailing the endonuclease reaction. $MgCl_2$, Influenza B RdRp heterotrimer, various amounts of inhibitor, and an activating RNA resembling the bound viral genome preincubated at 30 °C for 5 minutes. The reactions are then initiated via the addition of 5' Capped RNA. After, 8 minutes had elapsed the reactions were quenched.

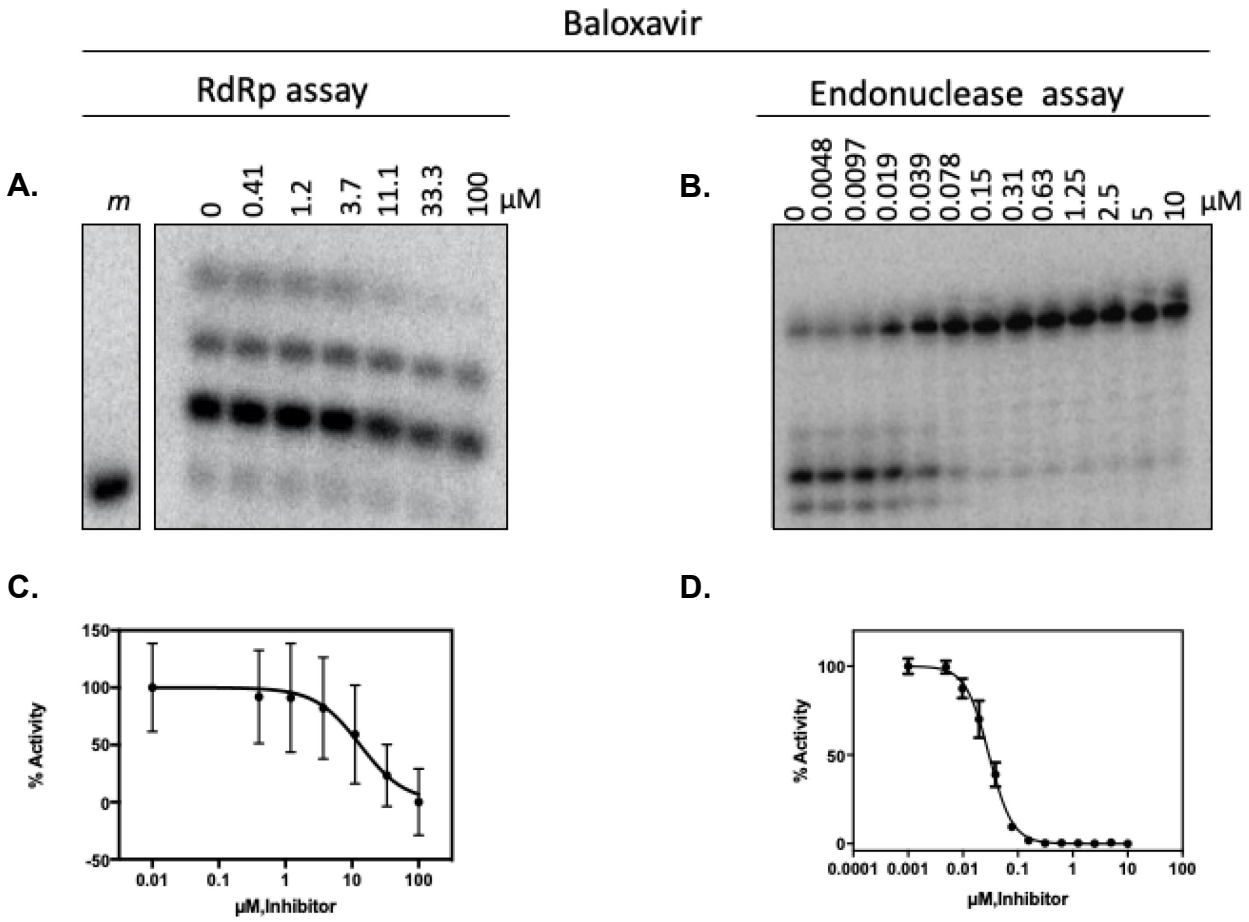

Figure 4.4: Baloxavir tested in Endonuclease and RdRp assay. The gel-based assay shows the titration of Baloxavir in RdRp assay up to 100 µM. m is the migration pattern of radiolabeled 14 nucleotides substrate, which serves as a marker. (B) The gel-based assay shows the titration of Baloxavir in Endonuclease assay up to 10µM. (C) & (D) The IC_{50} graph is represented by fitting quantified data from A and B. The error bars are based on at least three independent values.

Compound	Polymerase Assay IC50, µM	Endonuclease Assay IC50, µM
Baloxavir Acid	13	0.029

Table 4.1: The IC_{50} values obtained from RdRp and Endonuclease assay.

Chapter 5. Materials and Methods

5.1 Protein Expression & Purification

5.1.1 Development of the expression cassette

The construct, which is codon-optimized for protein production in insect cells, is synthetically synthesized (GenScript, Piscataway, NJ, USA) and integrated into the Baculovirus genome through a transformation through Tn7 transposition in E.Coli [67]. For transformation, we mixed 100ng of the plasmid with 100µL of chemically competent DH10EMBacY cells; then heat shocked the cells at 42ºC, which resulted in the plasmid being taken up by E.Coli. The next day, cells streaked out on LB-agar plates containing Kanamycin, Tetracycline, Chloramphenicol, Gentamycin, IPTG (1mM) and X-Gal for blue-white screening. White colonies harbour the integrated plasmid in the Baculoviral genome, re-streaking a white colony assures selecting the right colony. On the following day, a well-separated white colony used for starting a miniculture and then the miniculture used for initiating the first virus generation as explained in Garzoni et al in 2012 [67].

Using a commercially available plasmid preparation kit (QIAprep Spin Miniprep Kit), we alkaline lysed the bacteria. P1 solution is buffer with RNAse, P2 solution is alkaline lysis buffer and N3 neutralizing buffer added to the cells according to the manufacturer protocol. We centrifuged the solution and transferred the supernatant, which contains the virus to the fresh tube and centrifuged again, and then ethanol washed the pellet. The pellet was resuspended in 30 µl of sterile-filtered ddH2O and 200 µl of insect cell media. We used X-Treme Gene HP Transfection Reagent (Roche) for the transfection of insect cells (Sf9, Invitrogen, Burlington, ON, Canada). 1

million cells (Sf9, Invitrogen, Burlington, ON, Canada) were seeded in each well of a six-well tissue culture plate and transfected them with 100 µl of transfection solution according to manufacturer protocol. After 60 hrs, the supernatant was used to infect 50 ml of 1 million cells/ml and incubate it at 27ºC. To amplify the newly generated recombinant Baculovirus, the supernatant from these plates was used to infect a flask containing 50 ml of SF9 cells at a concentration of 10^6 cells/ml [74]. At 60 hours post infection, these cells were pelleted, and the supernatant collected. This solution contains the newly generated recombinant Baculovirus and is used for downstream protein expression.

5.1.2 Protein Expression

We used the Sf9 cell line (Gibco, Waltham, MA, USA) to express the influenza B polymerase complex. The cells were grown in Sf 900 II media (Gibco, Waltham, MA, USA). 5 µL of the recombinant Baculovirus was used to infect the 10^6 Sf9 cells. Four days post-infection, we measured cell density by using a 1:1 ration of cell culture and Trypan Blue and count the cells using Hemocytometer. The Trypan Blue dye helps in differentiation between live and dead cells (dead cells appears blue under the microscope), and as a result, we can calculate the cell viability. We then plot the cell growth graph using GraphPad Prism for the infected and non-infected cells. As an indicator of protein production Yellow Fluorescent Protein (YFP) was measured as Relative Fluorescence Unit (RFU), and the values were plotted using GraphPad Prism for both infected and non-infected cells. We then harvested the cells at day four.

5.1.3 Protein Purification

Infected cells were collected by centrifugation and resuspended in a lysis buffer consisting of Tris 100 mM, NaCl 1 M, EDTA 1 mM, TCEP 2 mM. The cells were also sonicated to ensure complete cell lysis. Cell debris was spun down at 30,000 RCF for 30 minutes. The supernatant was transferred to a new tube, and 1% w/v of Polyethylene Imine was added to precipitate the nucleic acids and centrifuged at 3,000 RCF for 15 minutes. We loaded the supernatant on the Strep-Tactin column (iba, Goettingen, Germany), and then, we washed the Strep-Tactin column with 60 Column Volume (CV) of 100 mM Tris, 1 M NaCl, 10% Glycerol, 1 mM EDTA, and 2 mM TCEP. Proteins were then eluted with 1X Elution Buffer (iba, Goettingen, Germany), 10% Glycerol, 2 mM TCEP. We then concentrated the protein preparation using a 50kDa concentrator and stored it at -20 °C in 50 mM Tris pH 8, 75 mM NaCl, 2 mM TCEP, and 45% Glycerol.

5.2 Gel-based Assay

5.2.1 Chemicals

We used 5'-phosphorylated RNA primer, 5'-p ACGC and templates, 5'-p UUUGUUCGCGU, 5'-p UUAUUUCAUGGCGU, symmetrical template symmetrical templates, 5'-pUUUCAUGGCGCGC, vRNA 5'-p AGUAGUAACAAGAGGGUAUUGUAUACCUCUGCUUCUGCU, and capped mRNA 5' N7MG-ppp-AAUCUAUAAUAGCAUUAUCC used in this study were purchased from Dharmacon (Lafayette, CO, USA). We purchased all NTPs from GE Healthcare (Cranbury, NJ, USA). α ^{32}P- CTP and α ^{32}P- GTP were purchased from PerkinElmer (Boston, MA, USA). All the NTPs were purchased from TriLink (San Diego, CA, USA).

5.2.2 RdRp Assay

We conducted the RNA synthesis assay with the mix of (final concentrations) Tris-HCl (pH 8, 25 mM), TCEP (2 mM), NaCl (20 mM) RNA primer (200 µM), RNA template (1 µM), α ^{32}P- NTP (0.1 µM), NTPs (1 µM), NTP analogues (100 µM), FluB RdRp complex (0.1 µM). The final volume of the reaction mixture was 15 µL and the mixture incubated for 10 minutes at 30 °C, and then the reaction started with $MnCl_2$ (2.5 mM). The reactions stopped after 30 minutes by adding 15 µL of formamide/EDTA (50 mM) mixture and followed by incubation at 5 °C for 10 minutes. Then, we loaded 3 µL in a 15% polyacrylamide denaturing gel electrophoresis, which consisted of 8 M Urea. As a result, it would resolve the RNA products into single strands. We then used phosphorimaging (Typhoon TRIP, variable mode imager, GE Healthcare Bio-Science, Uppsala, Sweden) to scan the gel and used ImageQuant 5.2 (GE Healthcare Bio-Science, Uppsala, Sweden) to quantify the bands.

5.2.3 Endonuclease Assay

We conducted the RNA endonuclease assay with the mix of (final concentrations) Tris-HCl (pH 8, 25 mM), NaCl (2.5 mM), vRNA (1.66 µM), FluB RdRp (0.05 µM) and $MgCl_2$ (5 mM). The final volume of the reaction mixture was 20 µL, and it was incubated for 10 minutes at 30 °C, and the reaction started by adding radiolabeled capped mRNA (0.1 µM). After 8 minutes, the reactions were stopped by adding 20 µL of formamide/EDTA (50 mM) mixture and followed by incubation at 95 °C for 10 minutes. Then we loaded 3 µL in a 15% polyacrylamide denaturing gel

electrophoresis, which consisted of 8 M Urea. We then used the same equipment and method for observation and quantification, as mentioned in RdRp assay.

5.2.4 Radiolabelling and Capping RNA

We used New England Biolabs Vaccinia Capping System (Fisher Scientific, Edmonton, Alberta, Canada) and α ^{32}P GTP (Perkin Elmer, Boston, MA, USA). We mixed RNA, vaccinia capping enzyme and α ^{32}P GTP and incubated for 30 minutes at 37 °C and at 95 °C for 10 minutes to stop the reaction by inactivation of the vaccinia capping enzyme. We then used GE Healthcare microspin G-25 columns (Chicago, IL, USA) and purified the radiolabeled and capped mRNA and then we extracted them by phenol-chloroform.

Chapter 6. Discussion

The RNA dependent RNA polymerase of RNA viruses is a promising target for antivirals. Inhibiting the RdRp directly decreases RNA synthesis. In influenza, the polymerase consists of three domains, each having a unique role in the process of genome replication and transcription. The functions of each of these domains can be targeted by antivirals, potentially providing new strategies in the fight against influenza.

In this study, we utilized an insect baculovirus based expression system to generate the RdRp of influenza B. To monitor the expression, we used a system by which YFP is co-expressed with the gene of interest. We then purified the protein complex using affinity chromatography. MS analyses confirmed the presence of all the subunits (PA/PB1/PB2) within the RdRp complex. To monitor the activity of the RdRp complex, we developed an assay utilizing a short model primer-template system [1]. In this system, the template allows for the incorporation of a radiolabelled NTP which serves as a signal source. We then chose a library of commercially available CTP analogues and screened them in the established assay. Here our data suggested that Arabinosyl CTP (araCTP) is able to compete with CTP and inhibits FluB RdRp. AraCTP or Cytarabine is an FDA approved cytotoxic drug which is used in treatment of acute myelocytic and acute lymphocytic [75], [76]. Our results suggest that araCTP selects only 23 times less than natural CTP; therefore, it is a good inhibitor of FluB polymerase. However due to high cell toxicity of the araCTP, it is not an optimal drug for treatment of the FluB.

Favipiravir is a broad-spectrum antiviral which is effective against negative and positive-sense RNA viruses [60]. However, studies show that it has teratogenic and embryotoxic effects [77]. In 2018, a study showed that continuous in-vitro passages lead to the PB1-K229R mutation in the influenza A virus that confers resistance to favipiravir. However, these mutant viruses are less fit

than the WT virus. As a result, the virus acquires PA-P653L to compensate for this loss of viral fitness [59]. We aligned the sequence of the influenza A strain that they used in their study with the influenza B strain sequence we used in our lab as well as other strains of influenza A, B, and C. The result obtained is aligned with other publications and shows that the K229R mutation is highly conserved among all different types of influenza. Studies on CVB3 also showed the K159R mutation in the F motif of the RdRp of the virus confers resistance to favipiravir [56]. We aligned the structure of the PB1 domain of FluB RdRp with the RdRp of the CVB3. Structural alignment of FluB with CVB3 shows that the lysine at position 229 in FluB is homologous to K159 CVB3.

It is important to study the key mutations that confer resistance to the current approved influenza virus antiviral. This gives us a better understanding of viral mutations and adaptations; therefore, we can utilize this understanding for the development of next-generation RdRp Inhibitors. To study resistance to favipiravir, we expressed and purified FluB PB1-K229R RdRp using the same approach as the WT enzyme. Using a model primer-template system, we were able to establish a biochemical assay to measure FluB WT and mutant enzyme kinetics. Overall, our data suggest that the K229R mutant shows a nine-fold decrease in Favipiravir incorporation. The K229R confers resistance to Ribavirin by five times in comparison with the wild-type enzyme. This is perhaps unsurprising given that ribavirin and favipiravir are structurally similar. Additionally, the K229R mutant showed no resistance to araATP, suggesting that the observed resistance is related to the structure of analogue.

We also tested the inhibition of the PA domain in a biochemical assay using FDA approved drug, Baloxavir Acid. This drug inhibits the endonuclease activity by chelating divalent-metal ion on the

active site of the PA subunit [66]. Because influenza RdRp has two active sites, we hypothesized that a divalent metal ion-chelator can bind and inhibit two active sites.

Based on our data, Baloxavir inhibits the endonuclease activity with IC_{50} of 0.029 µM, whereas, it inhibits the polymerase activity 448 times less with IC_{50} of 13 µM. Therefore, Baloxavir Acid seems to be a selective endonuclease inhibitor. This study may help the efforts to design new compounds and combinations that inhibit the endonuclease or RdRp active sites of the influenza RdRp.

References

[1] E. P. Tchesnokov, P. Raeisimakiani, M. Ngure, D. Marchant, and M. Götte, “Recombinant RNA-Dependent RNA Polymerase Complex of Ebola Virus,” *Sci. Rep.*, vol. 8, no. 1, pp. 1–9, 2018.

[2] A. Gordon and A. Reingold, “The Burden of Influenza: a Complex Problem,” *Curr. Epidemiol. Reports*, vol. 5, no. 1, pp. 1–9, 2018.

[3] R. G. Webster and E. A. Govorkova, “Continuing challenges in influenza,” *Ann. N. Y. Acad. Sci.*, vol. 1323, no. 1, pp. 115–139, 2014.

[4] M. Kuroda *et al.*, “Characterization of Quasispecies of Pandemic 2009 Influenza A Virus (A/H1N1/2009) by De Novo Sequencing Using a Next-Generation DNA Sequencer,” *PLoS One*, vol. 5, no. 4, 2010.

[5] D. R. Olson, L. Simonsen, P. J. Edelson, and S. S. Morse, “Epidemiological evidence of an early wave of the 1918 influenza pandemic in New York City,” *Proc. Natl. Acad. Sci. U. S. A.*, vol. 102, no. 31, pp. 11059–11063, 2005.

[6] P. R. Saunders-Hastings and D. Krewski, “Reviewing the history of pandemic influenza: Understanding patterns of emergence and transmission,” *Pathogens*, vol. 5, no. 4, 2016.

[7] B. Manz, M. Schwemmle, and L. Brunotte, “Adaptation of Avian Influenza A Virus Polymerase in Mammals To Overcome the Host Species Barrier,” *J. Virol.*, vol. 87, no. 13, pp. 7200–7209, 2013.

[8] J. C. Kwong *et al.*, “Acute Myocardial Infarction after Laboratory-Confirmed Influenza Infection,” *N. Engl. J. Med.*, vol. 378, no. 4, pp. 345–353, 2018.

[9] J. Monto, Arnold S. ; Gravenstein, Stefan ; Elliott, Michael ; Colopy,Michael ; Schweinle, “Clinical Signs and Symptoms Predicting Influenza Infection,” *Infect. Dis. Clin. Pract.*, vol. 10, no. 1, pp. 65–66, 2001.

[10] “Flu (influenza): For health professionals - Canada.ca.” [Online]. Available: https://www.canada.ca/en/public-health/services/diseases/flu-influenza/health-professionals.html. [Accessed: 12-Oct-2020].

[11] E. FODOR, “The RNA polymerase of influenza A virus: mechanisms of viral transcription

and replication E.," *Acta Virol.*, vol. 56, no. 2012, pp. 63–70, 2012.

[12] A. D. M. E. Osterhaus, G. F. Rimmelzwaan, B. E. E. Martina, T. M. Bestebroer, and R. A. M. Fouchier, "Influenza B virus in seals," *Science (80-.).*, vol. 288, no. 5468, pp. 1051–1053, 2000.

[13] E. A. Collin *et al.*, "Cocirculation of Two Distinct Genetic and Antigenic Lineages of," vol. 89, no. 2, pp. 1036–1042, 2014.

[14] D. Guilligay *et al.*, "Comparative structural and functional analysis of Orthomyxovirus polymerase cap-snatching domains," *PLoS One*, vol. 9, no. 1, 2014.

[15] S. Tong *et al.*, "A distinct lineage of influenza A virus from bats," *Proc. Natl. Acad. Sci. U. S. A.*, vol. 109, no. 11, pp. 4269–4274, 2012.

[16] W. H. O. Memorandum, "A revision of the system of nomenclature for influenza viruses: a WHO memorandum," *Bull. World Health Organ.*, vol. 58, no. 4, pp. 585–591, 1980.

[17] S. Tong *et al.*, "New World Bats Harbor Diverse Influenza A Viruses," *PLoS Pathog.*, vol. 9, no. 10, 2013.

[18] C. R. Parrish, P. R. Murcia, and E. C. Holmes, "Influenza Virus Reservoirs and Intermediate Hosts: Dogs, Horses, and New Possibilities for Influenza Virus Exposure of Humans," *J. Virol.*, vol. 89, no. 6, pp. 2990–2994, 2015.

[19] S. S. Lakdawala and K. Subbarao, "The challenge of flu transmission," *Nat. Med.*, vol. 18, no. 10, pp. 1468–1471, 2012.

[20] O. Munoz *et al.*, "Genetic adaptation of influenza a viruses in domestic animals and their potential role in interspecies transmission: A literature review," *Ecohealth*, vol. 13, no. 1, pp. 171–198, 2016.

[21] and R. J. W. M.F. Ducatez, R.G. Webster, "Animal influenza epidemiology," vol. 71, no. 2, pp. 233–236, 2013.

[22] "Shaw, M., and P. Palese. 2013. Orthomyxoviridae: the viruses and their replication. In: Knipe D.M., Howley P.M. (eds), Fields virology, 7th ed. Wolters kluwer/Lippincott Williams & Wilkins, Philadeplhia, PA. pp. 1152-1186

[23] I. T. Schulze, "Structure of the influenza virion," *Adv. Virus Res.*, vol. 18, no. C, pp. 1–55, 1973.

[24] K. Das, “Antivirals Targeting Influenza A Virus,” *J. Med. Chem.*, vol. 55, no. 14, pp. 6263–6277, 2012.

[25] S. Rao, A. C. Nyquist, and P. C. Stillwell, “Influenza,” *Kendig’s Disord. Respir. Tract Child.*, pp. 460-465.e2, 2018.

[26] Y. Shi, Y. Wu, W. Zhang, J. Qi, and G. F. Gao, “Enabling the ‘host jump’: Structural determinants of receptor-binding specificity in influenza A viruses,” *Nat. Rev. Microbiol.*, vol. 12, no. 12, pp. 822–831, 2014.

[27] R. W. Doms, A. Helenius, and J. White, “Membrane fusion activity of the influenza virus hemagglutinin. The low pH-induced conformational change,” *J. Biol. Chem.*, vol. 260, no. 5, pp. 2973–2981, 1985.

[28] I. M. Jones, P. A. Reay, and K. L. Philpott, “Nuclear location of all three influenza polymerase proteins and a nuclear signal in polymerase PB2.,” *EMBO J.*, vol. 5, no. 9, pp. 2371–2376, 1986.

[29] D. Dou, R. Revol, H. Östbye, H. Wang, and R. Daniels, “Influenza A virus cell entry, replication, virion assembly and movement,” *Front. Immunol.*, vol. 9, no. JUL, pp. 1–17, 2018.

[30] A. J. W. Te Velthuis and E. Fodor, “Influenza virus RNA polymerase: Insights into the mechanisms of viral RNA synthesis,” *Nat. Rev. Microbiol.*, vol. 14, no. 8, pp. 479–493, 2016.

[31] C. Liu, M. C. Eichelberger, R. W. Compans, and G. M. Air, “Influenza type A virus neuraminidase does not play a role in viral entry, replication, assembly, or budding.,” *J. Virol.*, vol. 69, no. 2, pp. 1099–1106, 1995.

[32] M. J. Rust, M. Lakadamyali, F. Zhang, and X. Zhuang, “Assembly of endocytic machinery around individual influenza viruses during viral entry,” *Nat. Struct. Mol. Biol.*, vol. 11, no. 6, pp. 567–573, 2004.

[33] S. Reich *et al.*, “Structural insight into cap-snatching and RNA synthesis by influenza polymerase,” *Nature*, vol. 516, no. 7531, pp. 361–366, 2014.

[34] C. Simpson and Y. Yamauchi, “Microtubules in influenza virus entry and egress,” *Viruses*, vol. 12, no. 1, pp. 1–20, 2020.

[35] J. S. Rossman and R. A. Lamb, “Influenza virus assembly and budding,” *Virology*, vol. 411,

no. 2, pp. 229–236, 2011.

[36] M. Breschkin, “Resistance of influenza viruses to neuraminidase inhibitors - a review,” *Antiviral Res.*, vol. 47, pp. 1–17, 2000.

[37] K. G. Nicholson, J. M. Wood, and M. Zambon, “Influenza,” *Lancet*, no. January, 2003.

[38] “WHO | Global Influenza Surveillance and Response System (GISRS),” *WHO*, 2020.

[39] A. S. Monto, “Reflections on The Global Influenza Surveillance and Response System (GISRS) at 65 Years: An Expanding Framework for Influenza Detection, Prevention and Control,” *Influenza and other Respiratory Viruses*, vol. 12, no. 1. Blackwell Publishing Ltd, pp. 10–12, 01-Jan-2018.

[40] F. Krammer and P. Palese, “Advances in the development of influenza virus vaccines,” *Nat. Rev. Drug Discov.*, vol. 14, no. 3, pp. 167–182, Mar. 2015.

[41] J. Owen Drife, “New England journal,” *Bmj*, vol. 318, no. 7197, p. 1565, 1999.

[42] F. Carrat and A. Flahault, “Influenza vaccine: The challenge of antigenic drift,” *Vaccine*, vol. 25, no. 39–40, pp. 6852–6862, 2007.

[43] C. Gerdil, “The annual production cycle for influenza vaccine,” *Vaccine*, vol. 21, no. 16, pp. 1776–1779, 2003.

[44] A. S. Monto, S. E. Ohmit, K. Hornbuckle, and C. L. Pearce, “Safety and efficacy of long-term use of rimantadine for prophylaxis of type A influenza in nursing homes,” *Antimicrob. Agents Chemother.*, vol. 39, no. 10, pp. 2224–2228, 1995.

[45] A. J. Hay, A. J. Wolstenholme, J. J. Skehel, and M. H. Smith, “The molecular basis of the specific anti-influenza action of amantadine.,” *EMBO J.*, vol. 4, no. 11, pp. 3021–3024, 1985.

[46] J. A. Mould *et al.*, “Influenza B virus BM2 protein has ion channel activity that conducts protons across membranes,” *Dev. Cell*, vol. 5, no. 1, pp. 175–184, 2003.

[47] Eton & LeporeRafal M. Pielak and James J. Chou, “Influenza M2 proton channels,” *Elsevier*, vol. 23, no. 1, pp. 1–7, 2010.

[48] “Influenza Antiviral Drug Resistance | CDC.” [Online]. Available: https://www.cdc.gov/flu/treatment/antiviralresistance.htm. [Accessed: 12-Oct-2020].

[49] “WHO Guidelines for Pharmacological Management of Pandemic Influenza A(H1N1) 2009

and other Influenza Viruses Part I Recommendations Pharmacological Management of Pandemic Influenza A (H1N1) 2009 Part I: Recommendations," 2010.

[50] M. Andres, "Mechanisms of resistance to neuraminidase inhibitors in influenza A viruses and evaluation of combined antiviral therapy," 2015.

[51] P. Koszalka, D. Tilmanis, and A. C. Hurt, "Influenza antivirals currently in late-phase clinical trial," *Influenza Other Respi. Viruses*, vol. 11, no. 3, pp. 240–246, 2017.

[52] K. Das, J. M. Aramini, L. C. Ma, R. M. Krug, and E. Arnold, "Structures of influenza A proteins and insights into antiviral drug targets," *Nat. Struct. Mol. Biol.*, vol. 17, no. 5, pp. 530–538, 2010.

[53] U. T.M., "Influenza diagnosis and treatment in children: A review of studies on clinically useful tests and antiviral treatment for influenza," *Pediatr. Infect. Dis. J.*, vol. 22, no. 2, pp. 164–177, 2003.

[54] J. A. L. Ives *et al.*, "The H274Y mutation in the influenza A/H1N1 neuraminidase active site following oseltamivir phosphate treatment leave virus severely compromised both in vitro and in vivo," *Antiviral Res.*, vol. 55, no. 2, pp. 307–317, 2002.

[55] Y. Furuta, B. B. Gowen, K. Takahashi, K. Shiraki, D. F. Smee, and D. L. Barnard, "Favipiravir (T-705), a novel viral RNA polymerase inhibitor," *Antiviral Res.*, vol. 100, no. 2, pp. 446–454, 2013.

[56] R. Abdelnabi, T. Silveira, and P. Leyssen, "Understanding the Mechanism of the Broad-Spectrum Antiviral Activity of Favipiravir (T-705): Key Role of the F1 Motif of the Viral Polymerase," vol. 91, no. 12, pp. 1–15, 2017.

[57] E. Takashita *et al.*, "Antiviral susceptibility of influenza viruses isolated from patients pre- and post-administration of favipiravir," *Antiviral Res.*, vol. 132, pp. 170–177, 2016.

[58] Z. Jin, L. K. Smith, V. K. Rajwanshi, B. Kim, and J. Deval, "The Ambiguous Base-Pairing and High Substrate Efficiency of T-705 (Favipiravir) Ribofuranosyl 5′-Triphosphate towards Influenza A Virus Polymerase," *PLoS One*, vol. 8, no. 7, pp. 1–10, 2013.

[59] D. H. Goldhill *et al.*, "The mechanism of resistance to favipiravir in influenza," *Proc. Natl. Acad. Sci.*, vol. 115, no. 45, pp. 11613–11618, 2018.

[60] E. Takashita, "Influenza Polymerase Inhibitors: Mechanisms of Action and Resistance,"

Cold Spring Harb. Perspect. Med., no. Table 1, p. a038687, 2020.

[61] H. Zhang *et al.*, "Novel influenza polymerase PB2 inhibitors for the treatment of influenza A infection," *Bioorganic Med. Chem. Lett.*, vol. 29, no. 20, p. 126639, 2019.

[62] E. J. Mifsud, F. G. Hayden, and A. C. Hurt, "Antivirals targeting the polymerase complex of influenza viruses," *Antiviral Res.*, vol. 169, no. June, p. 104545, 2019.

[63] E. Takashita *et al.*, "Susceptibility of influenza viruses to the novel cap-dependent endonuclease inhibitor baloxavir marboxil," *Front. Microbiol.*, vol. 9, no. DEC, pp. 1–7, 2018.

[64] T. Yang, "Baloxavir Marboxil: The First Cap-Dependent Endonuclease Inhibitor for the Treatment of Influenza," *Ann. Pharmacother.*, 2019.

[65] R. O'Hanlon and M. L. Shaw, "Baloxavir marboxil: the new influenza drug on the market," *Current Opinion in Virology*. 2019.

[66] S. Omoto *et al.*, "Characterization of influenza virus variants induced by treatment with the endonuclease inhibitor baloxavir marboxil," *Sci. Rep.*, vol. 8, no. 1, pp. 1–15, 2018.

[67] F. Garzoni, C. Bieniossek, and I. Berger, "The MultiBac BEVS for producing proteins and their complexes (Prot54)," *Epigenesys.Eu Protoc.*, no. February, 2012.

[68] G. Lu and P. Gong, "A structural view of the RNA-dependent RNA polymerases from the Flavivirus genus," *Virus Res.*, vol. 234, pp. 34–43, 2017.

[69] R. N. Kirchdoerfer and A. B. Ward, "Structure of the SARS-CoV nsp12 polymerase bound to nsp7 and nsp8 co-factors," *Nat. Commun.*, vol. 10, no. 1, pp. 1–9, 2019.

[70] L. Delang *et al.*, "Mutations in the chikungunya virus non-structural proteins cause resistance to favipiravir (T-705), a broad-spectrum antiviral," *J. Antimicrob. Chemother.*, vol. 69, no. 10, pp. 2770–2784, 2014.

[71] C. M. Lacbay, M. Menni, J. A. Bernatchez, M. Götte, and Y. S. Tsantrizos, "Pharmacophore requirements for HIV-1 reverse transcriptase inhibitors that selectively 'Freeze' the pre-translocated complex during the polymerization catalytic cycle," *Bioorganic Med. Chem.*, vol. 26, no. 8, pp. 1713–1726, 2018.

[72] S. Reich, D. Guilligay, and S. Cusack, "An in vitro fluorescence based study of initiation of RNA synthesis by influenza B polymerase," *Nucleic Acids Res.*, vol. 45, no. 6, pp. 3353–

3368, 2017.

[73] M. Lukarska *et al.*, “Structural basis of an essential interaction between influenza polymerase and Pol II CTD,” *Nature*, vol. 541, no. 7635, pp. 117–121, 2017.

[74] I. Berger, F. Garzoni, M. Chaillet, M. Haffke, K. Gupta, and A. Aubert, “The MultiBac Protein Complex Production Platform at the EMBL,” *J. Vis. Exp.*, no. 77, pp. 1–8, 2013.

[75] S. Cohen, “THE MECHANISMS OF LETHAL ACTION OF ARABINOSYL CYTOSINE (araC) AND ARABINOSYL ADENINE (araA),” 1976.

[76] R. D. Sundberg, F. Schaar, C. D. May, and V. Winkle, “B L 00 Nutritional,” vol. 27, no. 1, pp. 1143–1181, 2013.

[77] T. Furuta,Y., Komeno, T., & Nakamuba, “Polymerase Activity (%) 100 μ mol / L Favipiravir Favipiravir-RMP Control,” *Proc Jpn Acad Ser B Phys Biol Sci.*, vol. 93, no. 7, pp. 449–463, 2017.